1.80–1.75 Ga granite suites in the west Troms Basement Complex, northern Norway: Palaeoproterozoic magma emplacement during advancing accretionary orogeny, from field observations

S.G. Bergh, L. Haaland, Laurent Arbaret, N. Coint, M. Forien

1.80-1.75 Ga granite suites in the West Troms Basement Complex, northern Norway: Palaeoproterozoic magma emplacement during advancing accretionary orogeny, from field observations

Bergh, S.G.[1], Haaland, L.[1,4], Arbaret, L.[2], Coint, N.[3] and Forien, M.[1]

[1]University of Tromsø (UiT) – The Arctic University of Norway, 9037 Tromsø, Norway
[2] Université d'Orléans, ISTO, UMR 7327, 45071, Orléans, France
[3] Geological Survey of Norway, 7491 Trondheim, Norway
[4] Dept. of geoscience and petroleum, Norwegian University of Science and Technology, Trondheim, Norway
Corresponding author: Email address, steffen.bergh@uit.no (S.G. Bergh)

Abstract

The Ersfjord Granite is part of a suite of c.1.80-1.75 Ga syeno-granites in the West Troms Basement Complex, northern Norway, presumed to belong to the Transscandinavian Igneous Belt (TIB-1) in the Fennoscandian Shield. Previous data suggest the granite formed post-collisional and ascended as a batholite pluton from a source of sub-continental mantle and/or mafic-intermediate lower crust. We argue that the Ersfjord Granite was emplaced initially (c. 1.80 Ga) as multiple tabular sills in a back-arc extensional setting, then as successive melt injections (c. 1.78-1.75 Ga) in an evolving Andean/Cordilleran type accretionary orogen at the waning stages of the Svecofennian orogen. Field observations indicate melt ascent initiated as successive sills (EG-I) into well-foliated Meso/Neoarchaean TTG gneisses. Some sills preserved a magmatic layering, others injected and assimilated the host rock gneisses leaving pendants of mafic gneiss/migmatite residuum in between the granite sills. The first tectonic patches of melts (EG-II) ascended into the middle/upper crust along regional shear zones and injected into ductile imbricate thrust stacks (D1 event) during NE-SW directed crustal shortening and medium grade P-T conditions, using the sills and ancestor migmatite pendants as melt pathways. Then the tabular EG-I and II granite sheets and adjacent gneisses were coaxially folded by upright macro-folds (D2 event) and steep, granitic pegmatite dyke swarms (EG-III) intruded parallel to the fold axial surface and in related D2 thrusts, at low grade metamorphic conditions. The final melt emplacement (D3 event) included granite pegmatite dykes and sills (EG-IV) along subvertical D3 fold limbs and steep strike-slip shear zones. Our provisional back-arc and successive accretionary orogenic emplacement model for the Ersfjord Granite may explain ascent of many other TIB-1 magmas in the Fennoscandian Shield.

Commenté [LA1]: Batholith ?

Keywords

1.80-1.75 Ga TIB-1 related granites, sill intrusions, syn-tectonic thrust emplacement (D1), axial-planar dykes (D2), transpressive dykes (D3), back-arc extension, advancing accretionary orogen.

1. Introduction

Granites are widespread in the middle and upper continental crust from throughout the geological record, both as intrusive batholites, tabular sheets/sills, and discordant dykes in the host rocks (Vigneresse, 1995). One major site where juvenile continental crust grows and thickens is along convergent plate margins in advancing accretionary orogens associated with arc subduction (e.g., Condie, 2007; Cawood et al., 2009). Such orogens form when the overriding plate advances towards the downgoing plate causing repeated amalgamation of crustal fragments like magmatic arcs, rift/oceanic basins, volcano-sedimentary wedges, high- and low-pressure metamorphic rocks, and juvenile granitoid magmas, requiring strong mechanical coupling, localized strain in shear zones, and thermal rejuvenation (Cawood et al. 2009). Most petrological studies indicate that the primary source of granitoid melts in such orogens is from melting of mafic upper mantle rocks in magmatic arcs and/or back-arcs, and residual para- and ortho-gneisses and granulite/migmatites of the lower continental crust, and most likely melting occurred in a syn- to post-orogenic setting (Brown and Solar, 1998a; Sawyer et al., 2011). The processes however, by which continental margin crust is enriched in juvenile felsic magmas, i.e., the nature of segregation, extraction, and ascent of melt triggered by accretionary tectonism, are still uncertain (Brown and Rushmer, 2006; Brown, 2013).

The present paper addresses emplacement mechanisms of a major c.1.80-1.75 Ga, TIB-1 related syeno-granitoid magmatic suite in the Meso/Neoarchean to Palaeoproterozoic West Troms Basement Complex (WTBC), northern Norway (Figs. 1, 2; Bergh et al., 2010; Laurent et al., 2019). The WTBC accreted along the northwestern margin of the Fennoscandian Shield during the latest stages of the Svecofennian orogeny (Bergh et al., 2010, 2015), northeast of the high-pressure subduction-related juvenile magmatic arc in the Lofoten-Vesterålen area (Fig. 1; Griffin et al., 1978; Corfu, 2004, 2007). Previous workers consider the 1.80-1.75 Ga TIB-1 magmatism in WTBC as post-collisional and caused by lithospheric reworking (Laurent et al., 2019). We resolve how the widespread and repeated pulses of granitic magmas rather intruded as sills and partly assimilated the host rocks first in an area of extension with elevated heat flow, probably a back-arc setting, and then, in succession during convergent (D1-D3) ductile deformation in a small-scale advancing Andean or North American

Commenté [LA2]: I prefer «batholith» but sometime batholite is also found in english...as you want

Cordillera type accretionary orogen (cf. Cawood et al., 2009). We argue based on field observations, for syn-tectonic ascent and emplacement mechanisms of the granites, in a tectonic setting characterized by compressional shear zone strain typical of accretionary orogens (cf. Brown and Solar, 1998a, b; Vernon and Paterson, 2001; Weinberg and Mark, 2008).

2. Geological setting and previous work

2.1 The Fennoscandian Shield

The northern Fennoscandian Shield (Fig. 1) evolved through multiple Archaean orogenic and magmatic events (2.72-2.62 Ga) followed by Palaeoproterozoic rifting (2.5-2.0 Ga), and lastly by complex convergent, arc-accretion and collisional orogenic events at ca. 2.0-1.5 Ga including the Lapland-Kola, Svecofennian, Nordic, and Gothian orogenies (Hölttä et al., 2008; Lahtinen et al., 2005, 2008). These events resulted in crustal growth by amalgamation of an Archaean nuclei in the northeast and widespread Palaeoproterozoic accretionary growth towards the southwest (Kärki et al., 1993; Nironen, 1997; Åhäll and Connelly, 2008).

Archaean crust is present in the northeast of the Fennoscandian Shield overlain by a widespread Paleoproterozoic volcano-sedimentary basin cover formed during a period of major crustal extension at 2.5-2.0 Ga (Lahtinen et al., 2008; Bingen et al., 2015; Lahtinen and Köykkä, 2020). At c. 2.10 Ga the Archaean continent broke up and resulted in smaller terranes, e.g., the Karelian and Norrbotten provinces (Fig. 1). In the late Palaeoproterozoic interval most known Precambrian juvenile crust crystallized by arc-related magmatism (Daly et al., 2006; Condie, 2007; Cawood et al., 2009) during the Lapland-Kola (1.94-1.86 Ga), Svecofennian (1.92-1.79 Ga), and Nordic (1.78-1.75 Ga) orogens (Gorbatschev and Bogdanova, 1993; Lahtinen et al., 2008, 2009). In addition, the Transscandinavian Igneous Belt (1.87 Ga TIB-0 and 1.80-1.75 Ga TIB-1) formed during a major arc-magmatic episode that took place across the entire Fennoscandian shield (Larson and Berglund, 1992; Gorbatschev, 2004; Högdahl et al., 2004), and was followed by the Gothian orogeny (1.7-1.5 Ga) farther south in Scandinavia (Fig. 1; Gaál and Gorbatschev, 1987; Åhäll and Connelly, 2008). The Transscandinavian Igneous belt is trending NNW-SSE and intruded along the southwestern boundary of the Bothnian Basin of the Svecofennian domain, stretching. 2000 km across the entire southern part of Sweden

86 northward to Lofoten-Vesterålen and WTBC areas in northern Norway (Fig. 1; Corfu, 2004; Högdahl
87 et al., 2004).

88 Similar Archaean-Palaeoproterozoic basement provinces exist northwest of and within tectonic
89 windows of the much younger Caledonian orogen in northern Norway (Fig. 1). There, small volumes
90 of 1.87-1.86 Ga (TIB-0) intrusions exist in the Lofoten and Vesterålen areas (Fig. 1), in addition to
91 much more voluminous phases of TIB-1 related (c.1.80 Ga) granitoid magmas that belong to the
92 anorthosite-mangerite-charnockite-granite (AMCG) plutonic suite (Griffin et al., 1978; Corfu, 2004,
93 2007). Similar aged granites with a range of ages between 1.87 Ga, 1.80-1.75, and >1.63 Ga are
94 present on the islands of Senja and Kvaløya in western Troms, including the 1792 ± 5 Ma Ersfjord
95 Granite (Fig. 2; Andresen, 1979). The age of the Ersfjord Granite corresponds to the youngest, TIB-1
96 plutons (Högdahl et al., 2004) which formed coeval with late stages of the Svecofennian orogeny.
97 Other TIB-1 related c. 1.80 Ga monzo- and syenogranites crop out in the Rombak and Tysfjord
98 tectonic windows in the Caledonides south of Lofoten (Fig. 1; Andresen and Tull, 1986; Korneliussen
99 and Sawyer, 1989; Angvik et al., 2014). Additionally, several granitic suites dated at c.1.80 Ga are
100 present east of the Caledonian nappe front along strike with the WTBC (Slagstad et al., 2015). These
101 suites merge with A-type monzonitic, modern Andes type intrusive rocks in the Norrbotten province
102 of Sweden (Fig. 1; Bergmann, 2018), formed in a Cordillera type back arc setting by eastward
103 accretion/subduction associated with TIB-1 plutonic rocks farther west (e.g., Bergman et al., 2001;
104 Martinsson et al., 2018).

105 ## 2.2. The West Troms Basement Complex

106 The WTBC is a Meso-/Neoarchaean to Palaeoproterozoic province (Bergh et al., 2010) located west of
107 the Scandinavian Caledonides (Fig. 2; Roberts, 2003; Augland et al., 2014) and considered an
108 autochthonous part of the Fennoscandian Shield farther east (Fig. 1; Henkel, 1991; Olesen et al., 1997;
109 Bergh et al., 2012, 2014; Nasuti et al., 2015). The WTBC comprises TTG gneisses (2.92-2.6 Ga;
110 Myhre et al., 2013) present in three terranes or litho-tectonic segments; a northeastern segment with
111 juvenile (2.96-2.83 Ga) TTG granitoid rocks in Vanna and Ringvassøya, a southwestern segment of
112 sanukitoid type granitoids (2.71-2.69 Ga) in Senja, and an intervening segment on Kvaløya, with

remnants of 2.96 Ga, possible reworked TTGs (Fig. 2; Laurent et al. 2019). These crustal segments are separated by regional scale ductile shear zones like the Senja shear belt on Senja (Zwaan, 1995) and the Kvalsund shear zone on Ringvassøya (Fig. 2; Bergh et al., 2010). The host rock TTGs to the Ersfjord Granite on Kvaløya (Fig. 3) belong to the Gråtind Migmatite, Kattfjord Complex, Kvalsund Gneiss, and Bakkejord Diorite aged between 2.96 and 2.61 Ga (Zwaan, 1992; Corfu et al., 2003; Myhre et al., 2013). Main lithologies are tonalites, tonalitic gneisses, and migmatitic felsic and mafic gneisses (Zwaan, 1992; Armitage and Bergh, 2005; Bergh et al., 2010).

The Meso/Neoarchaean rocks in WTBC are assembled with several meta-supracrustal rift-related volcano-sedimentary sequences aged at 2.40-1.97 Ga (Myhre et al., 2011), mafic dyke swarms (2.4 and 2.2 Ga; Kullerud et al., 2006; Bergh et al., 2007; Paulsen et al., 2021), and granitoid and mafic igneous rocks in complex c. 1.80-1.75 Ga fold-thrust belt systems (Paulsen et al., 2021). The first juvenile magmatic pulse occurred at 1.87 Ga in Lofoten-Vesterålen (TIB-0) and was followed by 1.80-1.75 Ga TIB-1 related granites and diorites injected during multiple arc- and accretionary tectono-magmatic phases (D1-D3) in the WTBC (Andresen, 1979; Bergh et al., 2010; Laurent et al., 2019). Thus, magmatism linked to the Lapland-Kola orogen (1.94-1.88 Ga) and/or the early Svecofennian orogenic events (1.92-1.88 Ga) (cf. Daly et al., 2006; Lahtinen et al., 2008) are totally lacking in WTBC. The reason may be that the WTBC was separated and/or escaped deformation along the active Andes type Fennoscandian margin until TIB-related, 1.87 and 1.80-1.75 granites intruded due to westward progression of the orogenic deformation (1.78-1.75 Ga) toward the shield margin (Corfu et al., 2003; Bergh et al., 2015; Paulsen et al., 2021).

2.3 The Ersfjord Granite

The Ersfjord Granite (Andresen, 1979) belongs to the voluminous 1.80-1.75 Ga TIB-1 suite of monzo-/syeno-granite intrusions in the WTBC (Laurent et al., 2019), on the islands of Kvaløya and Senja (Fig. 2). Previous workers considered these granites to be post-collisional batholitic plutons (Laurent et al., 2019). In their model, the granites were largely undeformed and generated by post-tectonic delamination (e.g., Korja et al., 1993) of a deep-seated crustal root which formed earlier in the Svecofennian orogeny at c. 1.92-1.85 Ga (Laurent et al., 2019). Similar lithospheric reworking models

have been proposed for 1.80-1.75 Ga TIB-1 granitoids (Åhäll and Larson, 2000; Høgdahl et al., 2004; Gray and Pysklywec, 2012), but these models are not necessarily valid for the WTBC (this work), which account for a younger tectono-magmatic event with larger input of contaminated/ partially melted Archaean-Palaeoproterozoic crust (Laurent et al., 2019).

The present work shows that the Ersfjord Granite is not a single plutonic batholite, but rather intruded as sills and dykes in several tectonic pulses/events from c. 1.80 to 1.56 Ga, and termed EG-I to EG-V (see Table 1). These Ersfjord granite intrusions are all mostly massive, coarse-/medium-grained and porphyric, but locally also well foliated, with K-feldspar, plagioclase, quartz, primary biotite/ amphibole, epidote/-allanite, occasional muscovite, titanite, epidote, and Fe-Ti oxides/ magnetite, and accessory apatite and zircon (Laurent et al., 2019). Crystallization of the massive EG-I sills is previously dated at 1792 ±5 Ma, with metamorphic overprints at 1769±3 Ma and 1756±3 Ma (Andresen, 1979; Corfu et al., 2003), whereas similar massive, sill-like granites in Senja yielded ages between 1798 and 1784 Ma (Laurent et al., 2019), the latter thus marking the termination of the most voluminous of the TIB-1 granites in WTBC. Then, successive granite sills and dykes injected into the WTBC in Kvaløya synchronous with orogenic compression (c. 1.78-1.75 Ga), including W-E thrusting (D1), coaxial macro-folding (D2), orogen-parallel thrusting and lateral (transpressive) shearing (D3), and during post-orogenic reworking at 1.63-1.56 Ga (Bergh et al. 2015) (Table 1). In the foreland on Vanna Island, Paulsen et al. (2021) applied D1-D2 events, which correspond to D2-D3 in WTBC elsewhere.

Commenté [LA3]: Batholith?

3. Methods and data

Data used in this study (see Table 1) are from recent field and structural analyses by the authors and a master study (Haaland, 2018). Detailed structural analyses were made in Ersfjord Granite sills (EG-I), conformable granite-internal migmatite zones, and related melts in D1 ductile shear zones/thrusts (EG-II), and as melts in the foliation of adjacent TTG gneisses. Fully exposed contacts of the EG-I granite sills with TTGs were studied at Kjølen in the east and Tverrfjellet in the west (Fig. 3). Then we mapped and analyzed relative to host rock deformation, a D2 granite dyke swarm (EG-III) which intruded along axial-planar shear zones of upright D2 macro-folds at Otervika, c.10 km south of the

Commenté [LA4]: I'm not sure that a master report that cannot be easely found (it is ?) by readers will be accepted as a valid reference....In addition Haaland is co-author; therefore it is not necessary to cite this report...

main Ersfjord Granite body, and finally, resolved melt emplacement into subvertical D3 folds and strike-slip shear zones. The structural analysis involved determining the geometry of orogenic structures and kinematic characters of D1-D3 ductile shear zones that formed synchronous with EG-II to IV melt emplacement, and their relation to shortening strain and deformation patterns in the surrounding TTGs.

4. Results

The Ersfjord Granite in Kvaløya defines two large and several smaller, oblate- to lens-shaped, N-S to NW-SE trending geometric bodies arranged as several hundred granite sheets, or sills (Fig. 4a) parallel with the main foliation of surrounding TTG gneisses and metasupracrustal rocks (Fig. 3). The contacts with the host rocks are intrusive as in sills, except when they are reworked by D1 and D2 ductile thrusts (see below). Internally, these sills (EG-I) vary in thickness from ≤2 to c. 100 m, and typically are separated conformably by narrow mafic migmatite zones and superimposed ductile shear zones. Numerous smaller, and mineral-texturally similar granite sheets/sills, foliation-parallel lenses, and dyke swarms exist in the adjacent TTGs, e.g., in the Senja shear belt, in Kvalsund Gneiss east of Kaldfjord, in Kattfjord Complex gneisses at Otervika in southwestern Kvaløya, and in the Kvalsund shear zone on Ringvassøya (Figs. 2, 3).

4.1 Pre-tectonic sills (EG-I) and migmatite zones

The EG-I sills have an internally weak, but rhythmic, pervasive planar fabric composed of alternating coarse- and medium-grained granite with variable amount of aligned biotite and amphibole (Fig. 4b-c). This fabric dips gently both NE, NW, and north, but is mostly subparallel to sill contacts and foliation in the surrounding TTG gneisses and superposed D1-ductile shear zones (Fig. 3). The coarse- and medium-grained layers contain igneous textures with rectangular-shaped phenocrysts of perthitic feldspar and twinned plagioclase, with sharp grain contacts (Fig. 4d). Locally, aligned plagioclase phenocrysts yield a mineral lineation (Fig. 4e) which is plunging variably but mostly c. W-E. The layered fabric is often truncated and partly reorganized internally by felsic dykes with irregular contacts but similar texture and grain sizes as in the host EG-I sills (Fig. 4e).

Clusters and lenses of slightly aligned amphibolite pods exist as dismembered layers parallel to and inside thick EG-I sills, and the mafic and felsic components in combination, define a pseudo-layering (Fig. 5a-c). Locally, more fine-grained granites are seen as rim clusters around larger mafic pods (Fig. 5d). In addition to the mafic intercalations, extensive and prevalent, conformable mafic migmatite fabrics separate the EG-I sills and their distributed magmatic fabric. Such mafic migmatite zones are visible from a distance as regular depressions in between benches/ledges of the massive EG-I sills (Figs. 4a). The migmatite zones vary in thickness from <1m to 20 meters (Fig. 6a, b) and contain internally, fabric-parallel lenses and wedges of weakly layered EG-I sills with sharp to variously diffuse edges, and locally they are surrounded/cut by smaller, layer-oblique EG-I veins (Fig. 6c, d).

Distinct K-feldspar rich, red-colored granites that are petrographically and texturally similar to most EG-I sills (cf. Laurent et al., 2019) are also widely present in the surrounding Meso/Neoarchaean TTG gneisses farther west (Fig. 3) and in the Senja shear belt and Kvalsund shear zone (Fig. 2). In outcrops, such sills display sharp (intrusive) contacts and define rhythmic, massive and/or weakly layered granites in between tonalitic and mafic gneisses, whereas others have irregular and truncating, wedge-like contacts (Fig. 7b-d). Some sills are connected by discordant granite veins/clusters bifurcating into the mafic TTG gneiss foliation (Fig. 7b, c), others have irregular and locally boudinage contacts with the foliation of surrounding TTGs (Fig. 7e).

4.2 Syn-tectonic injections (D1-D3)

4.2.1. Granites injected in D1 ductile thrusts (EG-II)

Several generations of tectonic-related Ersfjord granitic melts (Table 1b-d) post-date the EG-I sill intrusions (cf. Bergh et al., 2010, 2015). We observed and defined the oldest tectonic melts (EG-II) as those that injected into migmatite zones in between EG-I sills and became themselves internally tightly folded, thrusted, and sigmoidal sheared (Figs. 8, 9, 10), thus defining ductile D1 shear zones.

The large-scale architecture of D1 shear zones is expressed as irregular, anastomosing EG-I sills and migmatite zones at Hollendaren (Fig. 3), where internal truncations define lenses, duplexes, and imbricate stack-like structures (Fig. 8a). Despite these irregularities, most D1 shear zones in the Ersfjord Granite overall are conformable with EG-I sills, migmatite zones, and foliation in the

surrounding TTGs (Fig. 3). Along the eastern contact between EG-I sills and Kvalsund Gneiss TTGs at Kjølen, sigmoidal-shaped granite (EG-II) define slices in a thrust-related duplex with top-to-the west displacement (Fig. 8b). Similar west directed D1 thrusts are mapped inside the main Ersfjord Granite body at Hatten and Store Blåmann (Fig. 3), comprising isoclinal D1 folds (Fig. 8c) with variably oriented fold axes that spread along an average shear zone girdle with strike mostly perpendicular to the main westerly shearing direction (Fig.11a). Stretching lineations are few, probably due to static metamorphic overgrowth on foliation surfaces, but reveal similar shear direction (Fig. 11a). The southwestern contact of the Ersfjord Granite with TTGs at Tverrfjellet (Fig. 3) is also a major thrust zone with top-to-the west sense of shear (Fig. 11a). This shear zone is up to 100 m thick and contains repeated, well-foliated granite lenses and aligned mafic pods in migmatite zones mostly conformable with the underlying TTG foliation.

In outcrops, EG-II sills in D1 shear zones are distinguished from EG-I sills in being overprinted by a ductile metamorphic foliation (Fig. 9a, b) which is distinguished from the magmatic fabric by presence of new-grown, syn-kinematic amphibole, flaky biotite, and locally garnet in a recrystallized quartz-feldspar matrix (Fig. 9c-f), suggesting mineral growth during shearing and amphibolite facies metamorphic conditions (see Table 1b). Strong foliation-internal elongation, boudinage, and lateral pinch-out of the EG-II sills and mafic pods can be seen along this foliation (Figs. 9b). The foliation wrapping around mafic pods are cut by both felsic EG-II vein-networks (Fig. 9a), and veins that are transposed and dismembered and often tightly folded by asymmetric, isoclinal and recumbent folds (Fig. 10a, b). Injected EG-II veins are present both along the axial-surfaces and limbs of such internal tight folds (Fig. 10c, d). All these observations of EG-II sills injected into D1 shear zones are summarized in Fig. 10e (see discussion).

Presumed D1 deformed EG-II sills are also widely observed along foliation of the surrounding TTG gneisses. Possible EG-II injections in TTGs include those granite sills that are internally displaced, thickened, transposed, and partly folded into the foliation, and tight to isoclinal folded and repeated granite veins in between thicker granite sills (Fig. 10f).

Commenté [LA5]: It is not clear in fig 10e what are the EGII layers with respect to EGI symbols. May be change the size or density of cross symbols for EGII...

4.3.2. Granites related to upright D2 macro-folds (EG-III)

A regional scale N-S to NW-SE trending D2 antiform exists between Ersfjord and Kattfjord (Armitage and Bergh, 2005) which folded all the TTGs and two metasupracrustal belts, and the Ersfjord Granite itself in Kvaløya (Figs. 3, 11b). Other major D2 folds are an antiform at Tverrfjellet (Figs. 3, 12), synformal folding of EG-I and -II sills between Hatten and Middagstind (Fig. 3), folds north and east of Kaldfjord, and a synform in the west at Otervika (Fig. 3). Notably illustrative is the D2 antiformal folding of the Tverrfjellet (D1) shear zone (Fig. 12a, b), shown by a change in dip direction on each fold limbs but consistent WSW-directed internal shear sense, thus demonstrating post-D1folding. At small-scale, D2 folds are asymmetric, and west-verging and they cut D1 foliation and EG-II sills at a high angle, and new EG-III sills are injected into these shear zones, and as separate dykes (Fig. 12c).

In the west at Otervika (Fig. 3) the TTGs and enclosed EG-I sills several tens of meters thick are folded by an open synformal D2 fold and cut by a widespread, axial planar granite pegmatite dyke swarm (EG-III) dipping moderately to the SW (Fig. 13a, b). One such pegmatite dyke which petrographically resembles coarse-grained varieties of EG-I sills, is previously dated at 1774 ± 5 Ma (Corfu et al., 2003). In outcrop the EG-III pegmatite dykes vary from planar to irregular, displaying abundant interconnected veins and straight contacts with the adjacent TTGs (Fig. 13b). The dyke contacts are mostly sharp and crosscut the D1 gneiss foliation and EG-I sills at high angle, but we observe injection of EG-III veins into the foliation of the mafic host gneisses as well as indentation of mafic gneiss layers into the EG-III pegmatites.

Similar D2 pegmatite dykes are present in TTGs of the Senja Shear Belt, and as irregular, transposed EG-III injections along several D2 axial-planer ductile thrusts in Kattfjord Complex gneisses north of Kaldfjord (Fig. 13c), adjacent to where the main Ersfjord Granite contact itself is a D2-related thrust (Fig. 3). A major, moderately east-dipping D2 shear zone is mapped at Buren (Figs. 3, 4a), which cuts EG-I and -II sills and differs from D1-thrusts in comprising massive EG-III sills transposed and altered to ortho-/ultramylonitic fabrics, but with same top-to-the west thrust sense (Fig. 13d). The mylonites consist of recrystallized, sigmoidal-shaped feldspar and quartz porphyroclasts, often surrounded by a matrix of S-C shaped flaky muscovite and biotite fishes (Fig. 13e). Additional growth

of aligned epidote, chlorite, and albite in mafic lenses of the shear zone at Buren addresses lower metamorphic conditions during the D2 event (i.e., greenschist facies) than for the D1 thrusting.

4.3.3. Granites injected in steeply plunging D3 folds and strike-slip zones (EG-IV)

A third group of structures into which Ersfjord granites injected are steeply NNE- to NW-plunging D3 macro- and meso-folds accompanied by subvertical NNE-SSW sinistral and NW-SE dextral strike-slip shear zones. The strike-slip shear zones are centimeter- to meter-thick, typically mylonitic, and oriented parallel to limbs and axial surfaces of steeply plunging D3 folds (Fig. 14a-c). Shear-sense estimates appear from drag-folding and ductile offset of D2 dykes (Fig. 14c, d), and by local subhorizontal stretching lineations. Macro-scale D3 folds reveal the same geometry and are inferred from refolding of D2 macro-folds at Tverrfjellet and east of Kaldfjord (Fig. 11b).

The D3 shear zones also comprise syn-kinematic injected granite pegmatite dykes and veins (EG-IV) texturally like D2 dykes, but more quartz- and K-feldspar rich (Table 1). An argument in support of D3 age for these dykes is that older EG-III dykes present in the adjacent TTG gneisses have been folded by similar, steeply NNE-plunging folds, and replaced by sheared granite veins (EG-IV) parallel to their axial surfaces (Fig. 14d).

Thin section studies of D3 shear zones show a typical mylonitic foliation consisting of sigmoidal lenses of saussuritized plagioclase clasts (albite), in a fine-grained matrix with syn-kinematic aggregates of recrystallized amphibole (now epidote + chlorite), biotite, and iron oxides (Fig. 14e), accounting for greenschist facies metamorphic conditions during D3.

4.3.4. Post-tectonic granite injections (EG-V)

The youngest felsic intrusions in the WTBC belong to a suite of post-D3 granite pegmatite dykes spanning ages between 1633 and 1562 Ma in the Astridal metasupracrustal belt in Senja (Bergh et al., 2015). Such pegmatites have patchy and jagged contacts with TTGs and are also found in Kvaløya where they crosscut all EG-I to -IV intrusions and are associated with quartz + biotite + muscovite + epidote mineral assemblages, as in Senja (Bergh et al., 2015).

5. Discussion

5.1 Pre-tectonic sill intrusion and emplacement (EG-I)

The Ersfjord Granite body is not a single batholithic pluton as previously assumed (Andresen, 1979; Bergh et al., 2010), but rather a set of regionally extensive tabular granite sills (EG-I). The thickest EG-I sills comprise a pervasive elongated fabric which we interpret as magmatic based on intergrowth of crystalline, rectangular feldspar phenocrysts, rhythmic banding/layering, and aligned texture of flaky biotite and hornblende (Figs. 4, 5). These textures may have developed by sheet/sill-internal flowage and/or in-situ local fractionation allowing magmatic layers to form in between already emplaced and newly injected sills (Table 1a). The granites possibly mixed with felsic components of the TTG crust, leaving trails of the mafic migmatite neosomes as rafts or pendant zones in conformable pseudo-layers (Fig. 5). This theory is verified by granite sills merging into and embedding mafic bodies (Figs. 5, 6), suggesting direct magma injection into the foliated host rocks (cf. Pawley et al., 2013). Such a mechanism would indicate upward transfer of voluminous granite melts as high-permeability magma sills into still viscous host rock TTGs (Fig. 7), and where the granite sills became separated from still solid leuco- and melanosome residuum layers (cf., Brown, 2010a, 2013).

Melting and emplacement of the huge amount of EG-I sills may have been triggered by high heat flow, for example in an extensional back-arc setting of the presumed evolving WTBC accretionary system. In this setting the vertical transfer of magma was large enough to segregate multiple, repeated and voluminous batches of melts that migrated into the upper crust along rheological weak fabrics (cf. Hyndman et al., 2005; Magee et al., 2018), such as Kvalsund shear zone and Senja shear belt. Then, several sheet-like pulses of magma ascended as extensive sills into the TTGs through the coalescence of either channelized magma segments, fingers, or lobes (Pollard et al., 1975; Schofield et al., 2010; Magee et al., 2016, 2018). Relatively small volumes of magma, however, formed compared to volumes in classic plutons attached to e.g., migmatite gneiss domes (e.g., Whitney et al., 2004).

5.2 Syn-tectonic D1 emplacement of sills during ductile thrusting (EG-II)

The onset of major NE-SW compression in the WTBC may have started after intrusion of EG-I granite sills at c. 1784-1774 Ma (Bergh et al., 2015; Laurent et al., 2019) in a presumed, closing back-arc system (cf. Silver et al., 1985). The tectonic-induced EG-II melts were channelized into D1 ductile thrusts subparallel with TTG gneiss foliation and ductile detachment faults (Table 1b) that controlled progressive supply of sill-like magmas (Magee at al., 2018). Crustal thickening by imbricate D1 thrusting then allowed new, smaller batches of EG-II magma to flow and reactivate the channels, while adjacent portions of the intrusion partly crystallized (cf. Holness and Humphreys, 2003; Currier and Marsh, 2015) and became folded and transposed in the D1 thrusts (Fig.10). These thrust-parallel veins and clusters of granite formed synchronously as interstitial melts that partly obliterated the relic mafic pendant fabric and re-melted the Neoarchaean TTG gneiss foliation. Magma injection and local re-melting of the TTGs synchronous with ductile deformation is supported by internal felsic net-veins (Fig. 9a) and may explain why renewed melt migration pathways remained operational over a large time frame (cf. Magee et al., 2016). Furthermore, preliminary age dating shows that the Neoarchaean TTG foliation in areas near main Ersfjord Granite bodies is late-Svecofennian (1.80-1.77 Ga) in age, and thus became fully overprinted and reworked by the regionally widespread D1-foliation (cf. Bergh et al. 2010, 2015; Myhre et al. 2013).

The ductile D1 event in WTBC triggered transfer of repeated EG-II granitic melts at amphibolite facies conditions synchronous with compressional, thrust-type deformation (Bergh et al. 2010). Our field data suggest that successive EG-II melts were formed and first used the relict migmatite pendant zones, then the D1 ductile thrusts and reworked TTG foliation as pathways for upward transfer of melts. A two-stage mechanism is favored, suggesting percolative flow of injected granite sills in the magmatic stage (Fig. 5), followed by viscous flow of melts channelized in the migmatite pendants which acted as ductile thrusts (Fig. 10) (cf. Brown and Solar, 1998b; Marchildon and Brown, 2003). A provisional ascent model is that new EG-II magmas were extracted by tectonic reworking and transferred upwards until they reached the near-solid state, foliation-parallel D1 thrusts at higher level in the crust. The granite melts then migrated into the ductile thrusts along hinges and axial surfaces of

recumbent isoclinal folds, causing transposition and layer disaggregation (Fig. 10). Thus, the driving force for ascent of new EG-II granite melts was likely strong and successive D1 ductile thrusting/ shearing and syn-tectonic flattening (cf. Vernon and Paterson, 2001; Weinberg and Mark, 2008). This occurred in a favorable NE-SW to E-W directed maximum D1 shortening field (Fig. 11a; Bergh et al., 2010), based on elongated and sheared mafic pods and boudins, sigmoidal lenses, tight isoclinal fold axes, and stretching lineations in D1 thrusts both inside reworked migmatite zones of the Ersfjord Granite and in adjacent TTG-gneisses (Fig. 10). The spread in D1 fold axes orientation (Fig. 11a) is likely due to strain-dependent reorientation within different D1 shear zones, controlled by their location relative to sill boundaries, thin versus thick sills, and/or internal pendant migmatite zones.

5.3. Late-tectonic D2 regional folding and dyke injection (EG-III)

The previous obtained age of 1774 ± 5 Ma for the granite pegmatite dykes at Otervika (Corfu et al. 2003) constrains the absolute timing of the D2 macro-folding (Table 1c). During this event, both the EG-I and II sills and surrounding TTG foliation were D2 folded and then EG-III injected as granite pegmatite dykes along the axial surfaces and in corresponding D2 thrusts (Figs. 12c, 13a, b). The D2 structures also developed by NE-SW to W-E directed maximum principal shortening (Fig. 11b), thus indicating that the D2 macro-folds, corresponding dyke swarm, and D2 thrusts resulted from coaxial crustal shortening relative to D1 (Bergh et al., 2010). The metamorphic conditions during D2, however, were slightly lower (upper greenschist facies), but still high enough to transport volatile granitic melts. The difference in metamorphic grade, and c. 10 Ma age span between EG-I and EG-III melts at Otervika (Table 1a, c) favor melt injection during two separate magmatic events, rather than one progressive D1-D2 shortening. Further, the volume of dyke magma injected during the D2 folding was much less, which may indicate waning granitic magmatism (melting) after c. 1784 Ma. This is supported by a lower frequency of EG-III dykes in TTGs compared to the number of EG-I and II sills.

The EG-III pegmatite dykes at Otervika classify as a composite, discordant body of regularly spaced dyke (swarm) with a high aspect ratio (Brown, 2013). Since the pegmatites injected both as dykes and thrusts parallel to the axial-surfaces of D2 folds (Fig. 12c), this suggest ascent of melts in compressional dykes (e.g., Brown, 2004, 2005, 2013), i.e., perpendicular to the regional shortening

direction (Fig. 11b). Similar strain-related ascent conduits are recorded in many convergent settings (Wickham, 1987; Lucas and St. Onge, 1995; Brown and Solar, 1998a; Vernon and Paterson, 2001; Weinberg et al., 2013). For example, where tabular granites that link deeper migmatite zones to shallower plutons are transported in dykes oriented at a high angle to the maximum shortening direction (Reichhardt and Weinberg, 2012; Brown, 2013). The EG-III melts were most likely emplaced along semi-ductile, crack-like deformation bands in D2 thrusts (Fig. 12c) (cf. Brown, 2004, 2005, 2010b) caused by external applied D2 shortening strain rather than by simple melt-internal (magmatic) over-pressure (Bons et al., 2001, 2004) or dilation in the crust.

The source of EG-III pegmatites is unknown, but an option is local re-melting of EG-I sills and subsequent ascent as melt portions into D2 dykes and thrusts. Arguments in support of re-melting is that isolated EG-III dykes merge out from EG-I sills in the TTGs (Fig. 7b-d). Therefore, and since just a small degree of partial melting is required to generate felsic pegmatites in convergent orogens, local re-melting is more likely than keeping the EG-I sills partial molten for >10 m.y.r.

5. 4. Late/post-tectonic D3 transpression and dyke injections (EG-IV and V)

The last deformation event (D3) in the WTBC records a strain history of transpression, with sub-vertical folding and orogen-parallel (NW-SE directed) strike-slip ductile shearing (Table 1d; Bergh et al., 2010; 2015). New-formed granite pegmatite veins, sills, and dykes (EG-IV) were injected as sills and dykes along steep TTG foliation, axial surfaces and limbs of subvertical D3 folds (Fig. 14a-d), and into steep ductile, left- and right slip D3 shear zones that offset D2-dykes (Fig. 14d). These shear zones suffered high strain, internal mylonitization and lateral displacement synchronous with emplacement of the EG-IV melts, still in the ductile regime, but at a slightly higher crustal level (lower greenschist facies conditions) than for the D1 and D2 events. Continued crustal uplift/ exhumation and injection of e.g., Rapakivi-like granites (Rämö and Haapala, 1995; Ernst et al., 2008) may explain the last granites (EG-V) injected in the WTBC, in the time span 1633-1562 Ma, likely due to post-orogenic, crustal reworking and rejuvenation (cf. Bergh et al., 2015).

5. 5. Regional implications and geotectonic model

The southwestern margin of the Fennoscandian Shield grew by accretion of juvenile arc-magmatic granitoids during the late-Svecofennian (c. 1.80 Ga), Nordic (c. 1.78-1.75 Ga) and Gothian (1.64–1.52 Ga) orogenies (Gaál and Gorbatschev, 1987; Lahtinen et al., 2008; Bingen et al., 2008). Farther northwest, the Ersfjord Granite in WTBC is coeval in age with the youngest granitoids of the Transscandinavian Igneous Belt (TIB-1), formed at c. 1.80-1.75 Ga during waning stages of a voluminous, late-Svecofennian arc-magmatic collisional event (Åhäll and Larson, 2000; Nironen, 1997; Ahl et al., 2001; Andersen et al., 2009; Andersson et al., 2004; Corfu, 2004; Gorbatschev, 2004; Högdahl et al., 2004). These TIB-1 granitoids are monzonitic and display I- to A-type geochemical affinities, attesting for melting of mafic to intermediate arc-like crust (Andersen et al., 2009; Andersson et al., 2004; Rutanen and Andersson, 2009) and/or mantle-derived crystalline melts (Skår, 2002). Since the same geochemical signatures were obtained for similar aged syeno-granitoids in the WTBC, a comparable source as for the TIB-1 granitoids was proposed (Laurent et al., 2019). The spatial link of the many other c. 1.80-1.75 Ga TIB-1 related granitoid magmatic suites in northern Norway (Griffin et al. 1978; Andresen and Tull, 1986; Korneliussen and Sawyer, 1989; Corfu 2004), and granitoids in the Norrbotten Province of Sweden farther east of the TIB belt (Fig. 1), suggests they may all be co-magmatic and back arc related (e.g., Bergman et al., 2001; Bergmann, 2018; Martinsson et al., 2018).

The Lofoten-Vesterålen AMCG suite intrusions, however, were emplaced mostly as massive plutons in a non-compressive (extensional) environment without large pendants of the host rocks (Griffin et al., 1979; Corfu, 2004, 2007; Coint et al., 2020), and presumably post-tectonic relative to the main Svecofennian Orogeny (cf. Laurent et al., 2019). Early arc delamination following NE-ward subduction at c. 1.80 Ga is proposed to have started in Lofoten slightly before or synchronous with crustal accretion and re-assembly of Neoarchaean crustal segments farther northeast, i.e., in the WTBC (Fig. 15a; Laurent et al., 2019). In this scenario, the 1.80 Ga Ersfjord Granite sills (EG-I), and granites in Senja intruded into TTGs in a back-arc extensional environment within the central TTG crustal segment on Kvaløya and bounding Neoarchaean shear zones (Senja shear belt, Kvalsund shear zone).

(Fig. 15a), i.e., pre-collisional relative to D1-D3 compressional events (Fig. 15b). A back-arc setting is the only region that can provide enough heat flow for long-term melting and ascent of the large granitoid EG-I sills in a setting adjacent to continental crust affected by compression (e.g., Hyndman et al., 2005; Currie and Hyndman, 2006; Currie et al., 2008).

The presence in WTBC of multiple crustal (TTG) segments, rift-related volcano-sedimentary sequences, fold-thrust belts, and intervening ductile shear zones into which juvenile mafic and felsic/granitoids (EG-II to IV) intruded (Bergh et al., 2010, 2015; Paulsen et al., 2021), account for continued shortening (D1-D3), amalgamation and melting in an advancing Andean or Cordilleran type accretionary orogenic setting (Fig. 15b). Such orogens are characterized by strong mechanical coupling and upper plate compression and transpression due to oblique assembly, crustal uplift, and thermal rejuvenation (cf. Cawood and Buchan, 2007; Cawood et al., 2009; Lallemand et al., 2005, 2008). Similar advancing accretionary events occurred in the WTBC (Fig. 15b, c), northeast of the Lofoten-Vesterålen magmatic arc, during the late- to post-Svecofennian collisional stages, and/or the Nordic and Gothian orogenies (cf. Lahtinen et al., 2008; Dallmeyer, 1992; Bergh et al., 2015). The bounding Senja shear belt and Kvalsund shear zone may have provided the sites of thermal and rheological weakening (cf. Sandiford et al., 2001), and thus were favorable pathways for the renewed ascending Ersfjord and Senja EG-II to IV granitoid melts (Fig.15b, c).

Our proposed advancing accretionary orogenic setting for emplacement of the Ersfjord Granite melts is supported by known melt ascent in both modern and ancient orogens (e.g., Brown, 1994; Petford et al., 2000). Modern examples include the North and South American Cordillera along the eastern Pacific, characterized by accretion and strike-slip motion of earlier rifted arcs and micro-continents, and formation of fold-thrust belts in retro-arcs (e.g., Johnston, 2001; Bergh, 2002; Lee et al., 2007; Cawood et al., 2009). Ancient examples are the Neoproterozoic to Palaeozoic Central Asian Orogenic Belt (Kröner et al., 2007; Windley et al., 2007), the juvenile Palaeoproterozoic Yavapai and Mazatzal provinces (Bergh and Karlstrom, 1992; Karlstrom et al., 2001), and Palaeoproterozoic orogens on the Australian craton (White et al., 2004; Collins and Sawyer, 1996). In all these accretionary orogens, granitic melts migrated through continental crust by compression, upward via structurally controlled

pathways like foliation and ductile, crustal shear zones (e.g., Brown, 2007, 2010a; Brown and Solar, 1998a, b, 1999), with ancestor melanosomes (White et al., 2004), and by granite melts associated with folds, boudins, and linear features (Collins and Sawyer, 1996).

5.6. Perspectives for future studies

Since Ersfjord Granite melts injected as sills (and dykes) both during pre-collisional extension and synchronous with convergent D1-D3 tectonic events, a direct spatial and temporal comparison of granitic magmas and ductile fabrics can be made. Our field-based approach provides an excellent basis for further geochronological and petrological-metamorphic studies (work in progress). Specific tasks would be: (1) U-Pb zircon dating of the EG-I through -IV generations of granitic sills and pegmatite dykes, and similar intrusions in the surrounding TTG gneisses, which is critical to genetically link the various melts. (2) Resolving the source of magma from geochemical signatures, e.g., mantle- or lower crust-generated (Laurent et al., 2019), and/or by partial melting of host rock gneisses. (3) Testing fluid-induced *in situ* melting/anataxis from a local source in the adjacent TTGs. (4) Isotopic studies of felsic and mafic melts in the migmatite pendant zones to be compared with leucosome and neosomes of migmatitic TTGs, to test if they are new Palaeoproterozoic melts, or remains of Neoarchaean migmaties. (5) Resolving the source and genesis of D2 and D3 granitic dykes, by re-melting of the pre-tectonic granite sills or from a fluid-enriched migmatite (TTG gneiss) source. 6) Establish the metamorphic history, P-T conditions and evolution of metamorphic minerals grown during the D1-D3 events. Such studies are valid to further test our local field-based granite emplacement model, and in evaluating magma sources and ascent of other TIB-1 granitoid intrusions both in the WTBC and comparable Fennoscandian Shield.

6. Conclusions

1) The Ersfjord Granite in the WTBC is not a single batholite body, but a system of tabular granite sills (EG-I) injected into Neoarchaean crustal segments (c. 1.80-1.78 Ga) triggered by pre-existing ductile shear zones and TTG fabrics in a back-arc extensional setting. The EG-I sills have an internal, distributed magmatic layering and rhythmic remains of Neoarchaean mafic migmatite pendant zones. The magmatic fabric of the sills developed during the melt/sill flowage and assimilation with the

surrounding, foliated TTGs, leaving irregular mafic migmatite pendants in conformable layers between the sills. These pendant zones acted as favorable conduits/pathways for later segregation and tectonic ascent of granitic melts.

2) New but smaller granite melts (EG-II) then formed and ascended syn-tectonically in a west-directed imbricate thrust nappes/stack (D1 event; 1.78-1.77 Ga) due to upper plate compression in an advancing Andean-type accretionary orogen. Thrust-parallel EG-II veins and clusters of granite channelized synchronously as interstitial melts that became sheared and partly obliterated the relic mafic pendant fabrics, at medium grade conditions.

3) Later, during a separate low grade tectono-magmatic event (D2; 1.774 Ga) granite pegmatite melts (EG-III) intruded as dyke swarms along the axial-surface of upright D2 macro-folds and in steep D2 thrusts, coaxial to D1 but higher in the accreted and thickened crust. Discordant EG-III dykes formed by compression at a high angle to the maximum D2 strain (NE-SW shortening), and not from melt overpressure. Still younger granite pegmatite melts (EG-IV) intruded along steep strike-slip shear zones and axial-surfaces of subvertical folds, in an orogen-parallel NW-SE shortening strain field (D3 event; c. 1.75 Ga).

4) The 1.80-1.75 Ga Ersfjord Granite suite in WTBC demonstrates granitoid magmatism and melt emplacement during pre-collisional back-arc extension, then continent closure and accretion(D1), coaxial shortening and crustal uplift (D2), transpressive reworking by oblique convergence (D3), and thermal rejuvenation (post-D3), in accord with an evolution history of a small-scale, advancing Andean and/or North American Cordillera type accretionary orogen.

Acknowledgements

The field-based data for this article were obtained through several years of study by the first author, and more detail structural analysis (MSci) undertaken by the second author, and by research partners at the Geological Survey of Norway and Université d'Orléans, France. The work is part of ongoing regional tectono-magmatic studies in the WTBC at UiT-The Arctic University of Norway. Financial support was achieved from UiT.

References

Åhäll, K.-I., Connelly, J. N., 2008. Long-term convergence along SW Fennoscandia: 330 my. of Proterozoic crustal growth. Precambr. Res. 161, 452-474.

Åhäll, K.I., Larson, S.Å., 2000. Growth-related 1.85–1.55 Ga magmatism in the Baltic shield: a review addressing the tectonic characteristics of Svecofennian, TIB 1-related, and Gothian events. GFF 122, 193–206

Ahl, M., Bergman, S., Bergström, U., Eliasson, T., Ripa, M., Weihed, P., 2001. Geochemical classification of plutonic rocks in central and northern Sweden: rapporter och meddelanden 106. Sver. Geol. Unders. 82.

Andersen, T., Andersson, U.B., Graham, S., Åberg, G., Simonsen, S.L., 2009. Granitic magmatism by melting of juvenile continental crust: new constraints on the source of Palaeoproterozoic granitoids in Fennoscandia from Hf isotopes in zircon. J. Geol. Soc. London 166, 233–247.

Andersson, U.B., Eklund, O., Claeson, D.T., 2004. Geochemical character of the mafic hybrid magmatism in the Småland-Värmland belt. Special Paper 37 In: Högdahl, K., Andersson, U.B., Eklund, O. (Eds.), The Transscandinavian Igneous Belt (TIB) in Sweden: A Review of Its Character and Evolution, Geological Survey of Finland, 47–55.

Andresen, A., 1979. The age of the Precambrian basement in western Troms, Norway. Geologiska Föreningen i Stockholm Förhandlingar, 101, 291-298.

Andresen, A., and Tull, J.F. 1986. Age and tectonic setting of the Tysfjord gneiss granite, Efjord, North Norway. *Norsk Geologisk Tidsskrift* 66, 69-80. ISSN 0029-196X.

Angvik, T.L., Bagas, L., Korneliussen, A., 2014. Geochemical evidence for arc-related setting of Paleoproterozoic (1790 Ga) volcano-sedimentary and plutonic rocks of the Rombak Tectonic Window. Manuscript in unpubl. PhD thesis, Structural development and metallogenesis of Paleoproterozoic volcano-sedimentary rocks of the Rombak Tectonic Window. UiT – The Arctic University of Norway.

Armitage, P. E., Bergh, S. G., 2005. Structural development of the Mjelde-Skorelvvatn Zone on Kvaløya, Troms: a metasupracrustal shear belt in the Precambrian West Troms Basement Complex, North Norway. Norw. J. Geol. 85, 117-132.

Augland, L. E., Andresen, A., Gasser, D., Steltenpohl, M. G., 2014. Early Ordovician to Silurian evolution of exotic terranes in the Scandinavian Caledonides of the Ofoten–Troms area – terrane characterization and correlation based on new U–Pb zircon ages and Lu–Hf isotopic data. Geol. Soc. London, Spec. Publ. 390, 655-678.

Bergh, S.G. 2002: Linked thrust and strike-slip faulting during Late Cretaceous terrane accretion in the San Juan thrust system, Northwest Cascades orogen, Washington. Geol. Soc. Am. Bull., 114, 934-949.

Bergh, S.G., Karlstrom, K.E., 1992. The Chaparral shear zone of central Arizona; deformation partitioning and heterogenous bulk crustal shortening during Proterozoic orogeny. Geol. Soc. American Bull, 104, 329-345.

Bergh, S.G., Kullerud, K., Corfu, F., Armitage, P.E.B., Davidsen, B., Johansen, H.W., Pettersen, T., Knudsen, S., 2007. Low-grade sedimentary rocks on Vanna, North Norway: a new occurrence of a Palaeoproterozoic (2.4–2.2 Ga) cover succession in northern Fennoscandia. Norw. J. Geol. 87, 301–318.

Bergh, S.G., Kullerud, K., Armitage, P.E.B., Zwaan, K.B., Corfu, F., Ravna, E.J.K., Myhre, P.I., 2010. Neoarchaean to Svecofennian tectono-magmatic evolution of the West Troms Basement Complex, North Norway. Norw. J. Geol. 90, 21–48.

Bergh, S.G., Corfu, F., Myhre, P.I., Kullerud, K., Armitage, P.E.B., Zwaan, C.B., Ravna, E.J.K., Holdsworth, R.H., Chattopadhya, A., 2012. Was the Precambrian basement of western Troms and Lofoten-Vesterålen in northern Norway linked to the Lewisian of Scotland? A comparison of crustal components, tectonic evolution and amalgamation history. Tectonics, In Tech Chapter 11, 283–330. https://doi.org/10.5772/48257.

Bergh, S.G., Kullerud, K., Myhre, P.I., Corfu, F., Armitage, P.E.B., Zwaan, K.B., Ravna, E.J.K., 2014. Archaean elements of the basement outliers west of the Scandinavian Caledonides in Northern Norway: architecture, evolution and possible correlation with Fennoscandia. In: Dilek, Y., Furnes, H. (Eds.), Evolution of Archean Crust and Early Life, Modern Approaches in Solid Earth Sciences 7, 103–126.

Bergh, S.G., Corfu, F., Priyatkina, N., Kullerud, K., Myhre, P.I., 2015. Multiple post-Svecofennian 1750–1560 Ma pegmatite dykes in Archaean-Palaeoproterozoic rocks of the West Troms Basement Complex, North Norway: Geological significance and regional implications. Precambr. Res. 266, 425–439.

Bergman, S., 2018. Geology of the Northern Norrbotten ore province, northern Sweden. Sveriges Geol. Unders., Rapporter och meddelanden 141, p. 430. ISBN 978-91-7403-393-9

Bergman, S., Kübler, L., Martinsson, O., 2001. Description of regional geological and geophysical maps of northern Norrbotten County (east of the Caledonian orogen). Sver. Geol. Und. Ba 56, 110 p.

Bingen, B., Andersson, J., Söderlund, U., Möller, C., 2008. The Mesoproterozoic in the Nordic countries. Episodes 31, 29–34.

Bingen, B., Solli, A., Viola, G., Torgersen, E., Sandstad, J.S., Whitehouse, M.J., Røhr, T.S., Ganerød, M., Nasuti, A., 2015. Geochronology of the Palaeoproterozoic Kautokeino Greenstone Belt, Finnmark, Norway: Tectonic implications in a Fennoscandia context. Norw. J. Geol. 95, 365-396.

Bons, P.D., Dougherty-Page, J., Elburg, M.A., 2001. Stepwise accumulation and ascent of magmas: J. Met. Geol. 19, 627–633, doi:10.1046/j.0263-4929.2001.00334.x.

Bons, P.D., Arnold, J., Elburg, M.A., Kalda, J., Soesoo, A., van Milligen, B.P., 2004. Melt extraction and accumulation from partially molten rocks: Lithos, 78, 25–42, doi:10.1016/j.lithos.2004.04.041.

Brown, M., 1994. The generation, segregation, ascent and emplacement of granite magma: The migmatite-to crustally-derived granite connection in thickened orogens: Earth Science Reviews, 36, 83–130, doi: 10.1016/0012-8252(94)90009-4

Brown, M., 2004. Melt extraction from lower continental crust: Transactions of the Royal Society of Edinburgh–Earth Sciences, 95, 35–48, doi:10.1017/S0263593300000900.

Brown, M., 2005, Synergistic effects of melting and deformation: An example from the Variscan belt, western France, in Gapais, D., Brun, J.-P., Cobbold, P.R., eds., Deformation Mechanism, Rheology and Tectonics: From Minerals to the Lithosphere: Geological Society of London Special Publication 243, p. 205–226.

Brown, M., 2007. Crustal melting and melt extraction, ascent and emplacement in orogens: Mechanisms and consequences: J. Geol. Soc. London, 164, 709–730, doi:10.1144/0016-76492006-171

592 Brown, M., 2010a Melting of the continental crust during orogenesis: The thermal, rheological and
593 compositional consequences of melt transport from lower to upper continental crust: Can. J. Earth Sci.
594 47, 655–694, doi:10.1139/E09-057.

595 Brown, M., 2010b, The spatial and temporal patterning of the deep crust and implications for the
596 process of melt extraction: Phil. Trans. Royal Soc. ser. A, 368, 11–51, doi:10.1098/rsta.2009.0200.
597
598 Brown, M., 2013. Granite: From genesis to emplacement. Geol. Soc. Am. Bull. 125, 1079–1113; doi:
599 10.1130/B30877.1

600 Brown, M., Solar, G.S., 1998a. Granite ascent and emplacement during contractional deformation in
601 convergent orogens: J. Struct. Geol. 20, 1365–1393.

602 Brown, M., Solar, G.S., 1998b. Shear zone systems and melts: Feedback relations and self-
603 organization in orogenic belts: J. Struct. Geol. 20, 211–227, doi:10.1016/S0191-8141(97)00068-0.

604 Brown, M., Solar, G.S., 1999. The mechanism of ascent and emplacement of granite magma
605 duringtranspression: A syntectonic granite paradigm: Tectonophysics, 312, 1–33, doi:10.1016/S0040-
606 1951(99)00169-9

607 Brown, M., Rushmer, T., 2006. Evolution and Differentiation of the Continental Crust: Cambridge,
608 UK, Cambridge University Press, 562 p.

609 Cawood, P.A., Buchan, C., 2007. Linking accretionary orogens with supercontinent assembly. Earth-
610 Science Reviews, 82, 217-256.

611 Cawood, P. A., Kröner, A., Collins, W. J., Kusky, T. M., Mooney, W. D., Windley, B. F., 2009.
612 Accretionary orogens through Earth history. In Cawood, P. A. Krøner, A. (eds:) Earth Accretionary
613 Systems in Space and Time. Geol. Soc. Lond. Spec. Publ. 318, 1–36. doi: 10.1144/SP318.1 0305-
614 8719/09/$15.00 .

615 Coint, N., Keiding, J.K., Ihlen, P.M. 2020. Evidence for Silicate–Liquid Immiscibility in Monzonites
616 and Petrogenesis of Associated Fe–Ti–P-rich rocks: Example from the Raftsund Intrusion, Lofoten,
617 Northern Norway. J. Petrol. 2020, 1–39. doi: 10.1093/petrology/egaa045

618 Collins, W.J., Sawyer, E.W., 1996. Pervasive magma transfer through the lower-middle crust during
619 noncoaxial compressional deformation: An alternative to diking: J. Met. Geol. 14, 565–579,
620 doi:10.1046/j.1525-1314. 1996.00442.x

621 Condie, K. C., 2007. Accretionary orogens in space and time. Mem. – Geol. Soc. Am. Bull. 200, 145.

622 Corfu, F., 2004. U–Pb Age, setting and tectonic significance of the AnorthositeMangerite-
623 Charnockite-Granite Suite, Lofoten-Vesterålen, Norway. J. Petrol. 45, 1799–1819.
624
625 Corfu, F. 2007. Multistage metamorphic evolution and nature of the amphibolite–granulite facies
626 transition in Lofoten–Vesterålen, Norway, revealed by U–Pb in accessory minerals. Chemical
627 Geology, 241, 108–128.

628 Corfu, F., Armitage, P.E.B., Kullerud, K., Bergh, S.G., 2003. Preliminary U–Pb geochronology in the
629 West Troms Basement Complex, North Norway: Archaean and Palaeoproterozoic events and younger
630 overprints. Bull. Geol. Surv. Norway. 441, 61–72.

631 Currier, R.M., Marsh, B.D., 2015. Mapping real time growth of experimental laccoliths: The effect
632 of solidification on the mechanics of magmatic intrusion: Jour. Volcanol.Geoth. Res. 302, 211–224,
633 doi: 10 .1016 /j .jvolgeores .2015 .07 .009.

Currie, C. A. and Hyndman, R. D. 2006. The thermal structure of subduction zone back arcs. Journal of Geophysical Research, 111, B08404, doi:10.1029/2005JB004024.

Currie, C. A., Huismans, R. S. and Beamont, C. 2008. Thinning of continental backarc lithosphere by flow-induced gravitational instability. Earth and Planetary Science Letters, 269, 436–447.

Dallmeyer, R.D., 1992: 40Ar/39Ar mineral ages within the Western Gneiss terrane, Troms, Norway: evidence for polyphase Proterozoic tectono-thermal activity (Svecokarelian and Sveco-norwegian). Precambr. Res. 57, 195-206.

Daly, J.S., Balagansky, V.V., Timmerman, M.J., Whitehouse, M.J., 2006. The LaplandKola orogen: Palaeoproterozoic collision and accretion of the northern Fennoscandian lithosphere. Geol. Soc. Lond. Mem. 32, 579–598.

Ernst, R.E., Wingate, M.T., Buchan, K.L., Li, Z.X., 2008. Global record of 1600–700 Ma Large Igneous Provinces (LIPs): implications for the reconstruction of the proposed Nuna (Columbia) and Rodinia supercontinents. Precambrian Res. 160,159–178.

Gaál, G., Gorbatschev, R. 1987. An outline of the Precambrian evolution of the Baltic Shield. Precambr. Res. 35, 15-52.

Gorbatschev, R., 2004. The Transscandinavian Igneous Belt – introduction and background, In: Högdahl, K., Andersson, U.B., and Eklund, O., eds. The Transscandinavian Igneous Belt (TIB) in Sweden: a review of its character and evolution: Geol. Surv. Finland, Spec. Paper, 37, 9–15.

Gorbatschev, R., Bogdanova, S. 1993, Frontiers in the Baltic Shield: Precambr. Res. 64, 3–21

Gray, R., Pysklywec, R.N., 2012. Geodynamic models of mature continental collision: evolution of an orogen from lithospheric subduction to continental retreat/delamination. J. Geophys. Res. 117 (B3), B03408.

Griffin, W.L., Taylor, P.N., Hakkinen, J.W., Heier, K.S., Iden, I.K., Krogh, E.J., Malm, O., Olsen, K.I., Ormaasen, D.E., Tveten, E., 1978. Archaean and Proterozoic crustal evolution in Lofoten-Vesterålen, N Norway. J. Geol. Soc. London 135, 629–647.

Haaland, L., 2018. Geometry and kinematic evolution of ductile shear zones in the Ersfjord Granite (1.79 Ga), West Troms Basement Complex: A Svecofennian accretionary thrust system. Unpubl. MSci thesis, UiT-The Arctic University of Norway. 71p.

Henkel, H., 1991. Magnetic crustal structures in northern Fennoscandia. Tectonophysics, 192, 57-79.

Holness, M., Humphreys, M., 2003. The Traigh Bhàn na Sgùrra sill, Isle of Mull: Flow localization in a major magma conduit: Journal of Petrology, 44, 1961–1976, doi: 10 .1093 /petrology /egg066.

Hyndman, R. D., Currie, C. A., Mazzotti, S. P. 2005. Subduction zone backarcs, mobile belts and orogenic heat. GSA Today, 15, 4–10.

Högdahl, K., Andersson, U.B., Eklund, O., 2004. The transscandinavian igneous belt (TIB) in Sweden: A review of its character and evolution. Geol. Surv. Finland Spec. Pap. 37, 125 p.

Hölttä, P., Balagansky, V., Garde, A., Mertanen, S., Peltonen, P., Slabunov, A., Sorjonen-Ward, P., Whitehouse, M., 2008. Archaean of Greenland and Fennoscandia. Episodes 31, 13–19.

Johnston, S. T. 2001. The Great Alaskan Terrane Wreck: Reconciliation of paleomagnetic and geological data in the northern Cordillera. Earth Plan. Sci. Letters, 193, 259–272.

678 Karlstrom, K. E., Ahall, K.-I., Harlan, S. S., Williams, M. L., MClelland, J., Geissman, J. W. 2001.
679 Long-lived (1.8–1.0 Ga) convergent orogen in southern Laurentia, its extensions to Australia and
680 Baltica, and implications for refining Rodinia. Prec. Res., 111, 5–30.

681 Koistinen, T., Stephens, M.B., Bogatchev, V., Nordgulen, Ø., Wennerström, M., Korhonen, J., Espoo,
682 Geol. Surv. Finland; Geol. Surv. Norway, Geol. Surv. Sweden, Ministry of Natural Resources of
683 Russia, Moscow 2001. Geological Map of the Fennoscandian Shield, Scale 1:2 000 000.

684 Korja, A., Korja, T., Luosto, U., Heikkinen, P., 1993. Seismic and geoelectric evidence for collisional
685 and extensional events in the Fennoscandian shield – implications for Precambrian crustal evolution.
686 Tectonophysics 219, 129–152.

687 Korneliussen, A., Sawyer, E. W., 1989. The geochemistry of Lower Proterozoic mafic to felsic
688 igneous rocks, Rombak Window, North Norway. Geol. Surv. Norw. Bull. 415, 7-21.

689 Kröner, A., Windley, B.F., Badarch, G., Tomurtogoo, O., Hegner, E., Jahn, B.M., Gruschka, S.,
690 Khain, E.V., Demoux, A., Wingate, M.T.D., 2007, Accretionary growth and crust formation in the
691 Central Asian Orogenic Belt and comparison with the Arabian-Nubian shield, in Hatcher, R.D., Jr.,
692 Carlson, M.P., McBride, J.H., and Martínez Catalán, J.R., eds., 4-D Framework of Continental Crust:
693 Geol. Soc. Am. Mem., 200, 181–209, doi: 10.1130/2007.1200(11).

694 Kullerud, K., Skjerlie, K. P., Corfu, F., de La Rosa, J. D., 2006. The 2.40 Ga Ringvassøy mafic dykes,
695 West Troms Basement Complex, Norway: The concluding act of early Palaeoproterozoic continental
696 breakup. Precambr. Res. 150, 183-200.

697 Lallemand, S., Heuret, A., Boutelier, D. 2005. On the relationships between slab dip, back-arc stress,
698 upper plate absolute motion, and crustal nature in subduction zones. Geochemistry, Geophysics,
699 Geosystems, 6, article number Q09006.
700
701 Lallemand, S., Heuret, A., Faccenna, C., Funiciello, F. 2008. Subduction dynamics as revealed by
702 trench migration. Tectonics, 27, doi:10.1029/2007/TC002212.
703
704 Larson, S. Å., Berglund, J., 1992. A chronological subdivision of the Transscandinavian Igneous
705 Belt—three magmatic episodes? Geol. För. Stockh. Förh. 114, 459-461.
706
707 Lee, C.-T.-A., Morton, D. M., Kistler, R. W., Baird, A. K. 2007. Petrology and tectonics of
708 Phanerozoic continent formation: From island arcs to accretion and continental arc magmatism. Earth
709 Plan. Sci. Letters, 263, 370–387.
710
711 Lahtinen, R., Köykkä, J., 2020. Multiply deformed Paleoproterozoic foreland fold and thrust belt in
712 northern Fennoscandia – The peripheral Kuusamo belt as a key example. Precambr. Res. 346, 105825

713 Lahtinen, R., Korja, A., Nironen, M., 2005. Palaeoproterozoic tectonic evolution of the Fennoscandian
714 Shield. In: Lehtinen, M., Nurmi, P., Rämö, T. (Eds.), The Precambrian Bedrock of Finland - Key to
715 the evolution of the Fennoscandian Shield. Elsevier Science B.V, 418–532.

716 Lahtinen, R., Garde, A. A., Melezhik, V. A., 2008. Paleoproterozoic evolution of Fennoscandia and
717 Greenland. Episodes, 31, 20-28.
718
719 Lahtinen, R., Korja, A., Nironen, M., Heikkinen, P., 2009. Palaeoproterozoic accretionary processes in
720 Fennoscandia, In: Cawood, P.A., Kröner, A. (Eds.), Earth Accretionary Systems in Space and Time.
721 Geol. Soc. London, Spec. Publ. 318, 237–256. DOI: 10.1144/SP318.8 0305-8719/09/

722 Laurent, O., Vander, J., Bingen, B., Bolle, O., Gerdes, A., 2019. “Building up the first continents:
723 Mesoarchean to Paleoproterozoic crustal evolution in West Troms, Norway, inferred from granitoid
724 petrology, geochemistry and zircon U-Pb/Lu-Hf isotopes. Precambr. Res. 321, 303–327.

725 Lucas, S.B., St. Onge, M.R., 1995. Syn-tectonic magmatism and the development of compositional
726 layering, Ungava orogen (northern Quebec, Canada): J.Struct. Geol., 17, 475–491, doi:10.1016/0191-
727 8141(94)00076-C.

728 Magee, C., Muirhead, J. D., Karvelas, A., Holford, S. P., Jackson, C. A. L., Bastow, I. D., Schofield,
729 N., Stevenson, C. T. E., McLean, C., McCarthy, W., Shtukert, O., 2016. Lateral magma flow in mafic
730 sill complexes. Geosphere 12, 809.

731 Magee, C., Stevenson, C.T.E., Ebmeier, S.K., Keir, D., Hammond, J.O.S., Gottsmann, J.H., Whaler,
732 K.A., Schofield, N., Jackson, C.A-L., Petronis, M.S., O’Driscoll, B., Morgan, J., Cruden, A., Vollgger,
733 S.A., Dering, G., Micklethwaite, S., Jackson, M.D., 2018. Magma Plumbing Systems: A Geophysical
734 Perspective. J. Petrol. 59, 1217–1251. 10.1093/petrology/egy064

735 Marchildon, N., Brown, M., 2003. Spatial distribution of melt-bearing structures in anatectic rocks
736 from southern Brittany: Implications for melt-transfer at grain to orogen-scale: Tectonophysics, 364,
737 215–235, doi:10.1016/S0040-1951(03)00061-1.

738 Martinsson, O., Bergman, S., Persson, P-O. Hellström, F.A., 2018. Age and character of late-
739 Svecokarelian monzonitic intrusions in northeastern Norrbotten, northern Sweden. In: Bergman, S.
740 (ed.). Geology of the Northern Norrbotten ore province, northern Sweden. Sveriges Geol. Unders.,
741 Rapporter och meddelanden 141, 380-399. ISBN 978-91-7403-393-9

742 Myhre, P.I., Corfu, F., Bergh, S.G., 2011. Palaeoproterozoic (2.0–1.95 Ga) pre-orogenic supracrustal
743 sequences in the West Troms Basement Complex, North Norway. Precambr. Res. 186, 89–100,
744 http://dx.doi.org/10.1016/j.precamres.2011.01.003

745 Myhre, P.I., Corfu, F., Bergh, S.G., Kullerud, K., 2013. U–Pb geochronology along an Archaean
746 geotransect in the West Troms Basement Complex, North Norway. Norw. J. Geol. 93, 1–24.

747 Nasuti, A., Roberts, D., Dumais, M.-A., Ofstad, F., Hyvönen, E., Stampolidis, A., Rodionov, A., 2015.
748 New high-resolution aeromagnetic and radiometric surveys in Finnmark and North Troms: linking
749 anomaly patterns to bedrock geology and structure. Norw. J. Geol. 95, 285-297.

750 Nironen, M., 1997. The Svecofennian Orogen: a tectonic model. Precambr. Res. 86, 21-44.
751
752 Olesen, O., Torsvik, T.H., Tveten, E., Zwaan, K.B., Løseth, H., Henningsen, T., 1997. Basement
753 structure of the continental margin in the Lofoten-Lopphavet area, northern Norway: constraints from
754 potential field data, on land structural mapping and palaeomagnetic data. Nor. Geol. Tidsskr. 77, 15–
755 30.
756 Paulsen, H-K., Bergh, S. G., Strmić Palinkaš, S., Karlsen, S.E., Kolsum, S., Rønningen, I. U.,
757 Armitage, P. E.B, Nasuti, A., 2021: Palaeoproterozoic foreland fold-thrust belt structures and lateral
758 faults in the West Troms Basement Complex, northern Norway, and their relation to inverted
759 metasedimentary sequences. Prec. Res., 362, 1-23, https://doi.org/10.1016/j.precamres.2021.106304

760 Pawley, M., Reid, A., Dutch, R. Preiss, W., 2013. A user’s guide to migmatites. Government of South
761 Australia. Report Book 2013/00016.

762 Petford, N., Cruden, A.R., McCaffrey, K.J.W., Vigneresse, J.L., 2000. Granite magma formation,
763 transport, and emplacement in the Earth’s crust: Nature, 408, 669–673, doi:10.1038/35047000
764

765 Pollard, D.D., Muller, O.H., Dockstader, D.R., 1975. The form and growth of fingered sheet
766 intrusions: Geol. Soc. Am. Bull, 86, 351–363, doi: 10 .1130 /0016 -7606 (1975)86 <351: TFAGOF>2
767 .0 .CO; 2.

768 Rämö, O.T., Haapala, I., 1995. One hundred years of Rapakivi granite. Mineral. Petrol. 52, 129–185.

769 Reichardt, H., Weinberg, R.F., 2012. Hornblende chemistry in meta- and diatexites and its retention in
770 the source of leucogranites: An example from the Karakoram shear zone, NW India: J. Petrol. 53,
771 1287–1318, doi:10.1093/petrology/egs017

772 Roberts, D., 2003. The Scandinavian Caledonides: event chronology, palaeogeographic settings and
773 likely modern analogues. Tectonophysics, 365, 283-299.

774 Rutanen, H., Andersson, U.B., 2009. Mafic plutonic rocks in a continental-arc setting: geochemistry of
775 1.87–1.78 Ga rocks from south-central Sweden and models of their palaeotectonic setting. Geol. J. 44,
776 241–279.

777 Sandiford, M., Hand, M. and McLaren, S. 2001. Tectonic feedback, intraplate orogeny and the
778 geochemical structure of the crust: A central Australian perspective. In: Miller, J. A., Holdsworth, R.
779 E., Buick, I. S. and Hand, M. (eds) Continental Reactivation and Reworking. Geol. Soc., London, Spec.
780 Publ., 184, 195–218.

781
782 Sawyer, E.W., Cesare, B., Brown, M., 2011. When the continental crust melts: Elements, 7, 229–234,
783 doi: 10.2113/gselements.7.4.229

784 Schofield, N., Stevenson, C., Reston, T., 2010. Magma fingers and host rock fluidization in the
785 emplacement of sills: Geology, 38, 63–66, doi: 10 .1130 /G30142 .1.

786 Silver, E.A., Ellis, M.J., Breen, N.A., Shipley, T.H., 1985. Comments on the growth of accretionary
787 wedges. Geology, 13, 6–9. https://doi.org/10.1130/0091-7613

788 Skår, Ø., 2002. U-Pb geochronology and geochemistry of early Proterozoic rocks of the tectonic
789 basement windows in central Nordland, Caledonides of north-central Norway. Precambr. Res.116,
790 265–283.

791 Slagstad, T., Willemoes-Wissing, B., Coint, N., Stampolidis, A., Ganerød, M., Ofstad, F., 2015.
792 Geology and metallogenic potential of the northwesternmost Norrbotten Province around Altevatn in
793 Troms, northern Norway. Norw. J. Geol. 95, 445-466. http://dx.doi. org/10.17850/njg95-3-07.
794
795 Vernon, R.H., Paterson, S.R., 2001. Axial-surface leucosomes in anatectic migmatites:
796 Tectonophysics, 335, 183–192, doi:10.1016/S0040-1951(01)00049-X.

797 Vigneresse, J.-L., 1995. Crustal regime of deformation and ascent of granitic magma: Tectonophysics,
798 249, 187–202, doi:10.1016/0040-1951(95)00005-8.

799 Weinberg, R.F., Mark, G., 2008. Magma migration, folding, and disaggregation of migmatites in the
800 Karakoram shear zone, Ladakh, NW India: Geol. Soc. Am. Bull. 120, 994–1009, doi:10.1130
801 /B26227.1.

802 Weinberg, R.F., Regenauer-Lieb, K., 2010. Ductile fractures and magma migration from source:
803 Geology, 38, 363–366, doi:10.1130/G30482.1.

Weinberg, R.F., Hasalová, P., Ward, L., Fanning, C.M., 2013. Interaction between deformation and magma extraction in migmatites: Examples from Kangaroo Island, South Australia: Geol. Soc. Am. Bull., 124, 000–000, doi:10.1130/B30781.1

White, R.W., Powell, R., Halpin, J.A., 2004. Spatially focused melt formation in aluminous metapelites from Broken Hill, Australia: J. Met. Geol. 22, 825–845, doi:10.1111/j.1525-1314.2004.00553.x

Whitney, D., Teyssier, C., Vanderhaeghe, O., 2004. Gneiss domes and crustal flow. Geol. Soc. Am. Spec. Paper 380, 15-33.

Wickham, S.M., 1987. The segregation and emplacement of granitic magma: J. Geol. Soc. London,144, 281–297, doi:10.1144/gsjgs.144.2.0281.

Windley, B. F., Alexeiev, D., Xiao, W., Kröner, A. and Badarch, G. 2007. Tectonic models for accretion of the Central Asian Orogenic Belt. Journal of the Geological Society, London, 164, 31–47.

Zwaan, K.B., 1992. Database for alle geologiske opplysninger om den prekambriske geologien på Kvaløya, Troms fylke. Geol. Surv. Norway, Report series, 92-104.

Zwaan, K. B. 1995: Geology of the Precambrian West Troms Basement Complex, northern Norway, with special emphasis on the Senja Shear Belt: a preliminary account. Geol. Surv. Norw. Bull. 427, 33-36.

Zwaan, K.B., Fareth, E., Grogan, P.W., 1998. Bedrock Map Tromsø, Scale 1:250 000. Geological Survey of Norway.

Figure captions

Figure 1. Overview geological map of the Fennoscandian Shield showing the Archaean Kola, Karelian and Norrbotten cratons, timing of major Palaeo- and Mesoproterozoic tectonic events (Lapland-Kola, Svecofennian and Gothian orogens), plutonic rocks of the Transscandinavian Igneous belt, and regional ductile shear zones (from Koistinen et al., 2001 and Bergh et al., 2015). Note location of the West Troms Basement Complex and Lofoten-Vesterålen areas to the northwest of the Paleozoic Caledonian Orogen. Abbreviations: BSSZ=Bothnian-Senja shear zone, MOL=Malangen-Onega lineament, R=Rombaken, RLZ=Raahe-Ladoga shear zone, Tys=Tysfjord, TIB=Transscandinavian Igneous Belt, WTBC=West Troms Basement Complex.

Figure 2. Geological and structural overview map with cross-section of the West Troms Basement Complex, after Bergh et al. (2010) and Paulsen et al., (2021). The Ersfjord Granite bodies are in the middle part of the complex, on the island of Kvaløya.

Figure 3. Geological and structural map of the Ersfjord Granite suite and the surrounding host rock TTG gneisses and metasupracrustal belts in Kvaløya, with interpreted cross-section. Mapped structures include foliation in the TTG gneisses, and traces of migmatite pendant zones and D1 ductile shear zones inside the Ersfjord Granite. Note also the Tverrfjellet shear zone (TSZ), D1 and D2 shear zones at Buren, and upright macro-folds (D2). Map is modified from Zwaan et al. (1998), Bergh et al. (2010), and Haaland (2018). Abbreviations: Msb=Mjelde-Skorelvvatn belt, Stb=Steinskardtind belt.

Figure 4. a) Panorama view of the main Ersfjord Granite body between Buren and Store Blåmann (see location in figure 3) showing internal tabular fabric dipping gently NW and defining light-colored sheets/sills (EG-I). b) Close-up view of EG-I granite sill with thin-laminated layers and uniform rhythmic banded, dark biotite-hornblende rich granite. Locality, Hatten. c) Magmatic layers of coarse-grained K-feldspar and biotite-hornblende-rich EG-I granite in irregular lens-shaped arrangement within the distributed magmatic fabric. Locality, Store Blåmann. d) Sharp contact between coarse- and

fine-grained EG-I granite layers. Note weak aligned fabric in fine-grained part, whereas the coarse-grained layer has a uniform texture of phenocryst feldspar and quartz. Locality, Store Blåmann. e) Coarse-grained EG-I granite with a distributed magmatic fabric of aligned, porphyric K-feldspar grains defining a mineral lineation in a matrix of biotite, hornblende, and plagioclase. Note discordant EG-I dyke truncating the aligned magmatic fabric with irregular character and similar texture and grain size as in the aligned mineral fabric. Locality, Store Blåmann.

Figure 5. Field examples of EG-I granite sills with mafic intercalations. a-b) Road-cut section with sketch interpretation showing coarse-grained EG-I sills. Note irregular lenses and clusters of mafic/amphibolitic pods (dark grey shade) embedded in the granite sills. Locality; south of Grøtfjord. c) Lenses and intercalations of aligned mafic pods within EG-I sill, defining pseudo-layers. Locality, Hatten. d) Massive EG-I granite sill with isolated mafic lenses and pods (dark grey) that are slightly elongated. Note light-colored granite rims around individual mafic pods. Locality; Buren.

Figure 6. a) Outcrop photograph of repeated mafic migmatite zones conformable with massive EG-I sills in the mountain Hatten. b) Section through a migmatite zone at Hatten, with textural details including (c, d) decimeter to meter-thick wedge-shaped, biotite-rich EG-I sills and inter-layered, partly dismembered mafic migmatite gneisses and pods. Hammer for scale is circled yellow.

Figure 7. Photos of presumed EG-I granites injected as sills into the surrounding TTG gneisses. a) Foliation-parallel K-feldspar rich granite layer/sill in mafic TTGs. Locality, Senja shear belt south of Astridal belt (see location in figure 2). Note aligned hornblende defining planar fabric in the granite. b) Series of TTG gneisses intruded by conformable, massive coarse-grained granite sills. Note sharp sill contacts and discordant linkage of small granite vein (dyke) between the two granite layers. Locality: Kvalsund shear zone on Ringvassøya. c) Coarse-grained granite cluster which bifurcates into the foliation of mafic TTGs, in Kvalsund shear zone. d) Massive and coarse-grained granite arranged as wedge-shaped sills around well-foliated mafic gneisses. Locality; Kvalsund shear zone. e) Series of TTG gneisses with foliation-parallel granite layers/sills, one which comprises boudinage (center of photo) and cut by a younger granite dyke (D2) (upper right in photo).

Figure 8. a) Photo of mountainside below Hollendaren (see location in figure 3), showing EG-I granite sills with an irregular attitude and variable dips, defining internal imbricates and duplex-like structures. Sense-of shear is to the west (left) as apparent from duplex geometries (in center of photo). b) Contact zone between the main Ersfjord Granite body and Kvalsund Gneiss at the mountain Kjølen. Sigmoidal lenses of granite (EG-II) and intercalated amphibolite gneisses are mixed in a ductile thrust system with top-to-the-west shear sense. Geographic location: 69º44’43’’N, 18º46’11’’E. c) Close-up view of injected EG-II granite slice and TTG gneiss along thrust surface in figure 9b. Note isoclinal fold and transposed EG-II lenses in mica-rich ductile shear fabric.

Figure 9. a) Details from a mafic migmatite zone in between EG-I sills, which is injected by irregular EG-II granite sills (lower part of photo) with internal vein-networks (in center of photo) parallel to a weak ductile foliation (D1). Locality; Buren. b) Mafic migmatite zone with aligned, variously dismembered EG-II sheets/sills of granite injected parallel to a foliation (D1), some surrounding mafic pods. Locality; Store Blåmann. c, d) Thin-section image of foliated biotite-rich EG-II granite sill (as in 9b) showing granoblastic microcline, albite, and quartz in a well-defined lepidoblastic biotite D1 oliation (D1). e, f) Thin section image of foliated mica-rich granite gneiss with garnet porphyroblast in mica-rich D1 foliation. Locality; Tverrfjellet shear zone. Images are shown in cross-polarized light (c, e) and plane-polarized light (d, f).

Figure 10. Outcrop photographs of syn-tectonic EG-II sills and veins within migmatite zones reworked as D1 ductile shear zones. a) Coarse-grained EG-II veins injected along D1 foliation and isoclinally folded. Locality: Hatten, 69º40’44’’N, 18º32’52’’E. b) Multiple coarse-grained EG-II granite sills that are internally folded by isoclinal folds and transposed, dismembered, and embedded axial-planar into

the main D1 foliation (D1). Locality; Hatten. c) Asymmetric fold in D1 shear zone that folds light-colored EG-I layers and is cut by EG-II granite along the axial-surface (black arrow). Locality; west of Buren, 69º42'59''N, 18º36'01E. d) Outcrop from same shear zone as 10c, showing asymmetric folded, sheared, and imbricated mafic gneiss lenses cut by EG-II sills along axial surfaces of the folds and along imbricate D1 shear foliation surfaces. e) Sketch summary of observations in figure 10c, d from Hatten. f) Presumed EG-I or II granite sills defining layers parallel to foliation in mafic TTGs, and which are themselves internally folded and truncated by new granite veins along fold axial surfaces. Locality; Senja shear belt.

Figure 11. Lower-hemisphere stereo-nets showing structural orientation data for the main D1 and D2 event features in key areas within and outside the main Ersfjord Granite bodies. a) D1 ductile shear zone foliation outlined as single great circles, average orientation, and poles. Separate D1 stereo-plots below are from key localities at Tverrfjellet, Hatten, and Buren. Great circles display an average D1 shear zone orientation for each locality, with enclosed D1 fold axis orientations, and stretching lineations. Note the large spread in trend of measured fold axes along average D1 shear zones, whereas stretching lineations vary less, between WNW and WSW. b) Orientation data for D2 macro-folded D1 foliation (great circles and poles) in Tverrfjellet shear zone, TTGs at Tverrfjellet and between Mjelde-Skorelvvatn and Steinskardtind supracrustal belts, and from D1 and D2 shear zones at Buren. Local D2 fold axis orientations are obtained from constructed β-axes. Note that variations in D2 fold axial surfaces infer refolding by large-scale D3 folds.

Figure 12. Panorama view (a) and interpretation (b) of the D2 folded Tverrfjellet shear zone and overlying EG-II Ersfjord Granite sills at the contact with Gråtind Migmatite TTGs southwest of Middagstind (see figure 3 for location). Note intrafolial D1 folds and sigmoidal mafic pods and EG-II lenses in Tverrfjellet shear zone with consistent top-SW shear sense, and the slightly discordant contact to TTGs below. Above the Tverrfjellet shear zone, multiple and conformable D1 shear zones alternate with massive EG-I sills. c) Sketch summarizing features related to D2 macro-folds in TTGs at Otervika. Note axial-planar D2 thrust with injected EG-III veins and associated thrust-related folds (at Buren), and injected EG-III dykes (see details in figure 13).

Figure 13. a) Macro-scale D2 synform that folds EG-I sills and the surrounding Kattfjord Complex TTGs at Otervika (see location in figure 3) and showing granitic pegmatite dykes (EG-III) intruded along the axial surface of the fold. Note regular dip of the dykes to the SW (right). b) Outcrop photograph of EG-III granite pegmatite dykes that crosscut foliated TTGs along road-cut in 13a. Note regular orientation of some dykes, complex splay geometries of subsidiary dykes, and locally irregular and bifurcating contacts indicating shearing along dyke contacts. The foliation of TTGs dips left (NE) and comprise internal EG-II veins. c) EG-III granite dykes injected at high angle with D1 foliation in Kattfjord Complex gneisses and along the axial surface of asymmetric D2 meso-folds. Note irregular and transposed EG-III veins caused by injection during thrusting. Locality: 1 km north of Kaldfjord (see location in figure 3). d) Details from a mylonitic D2 shear zone with EG-III granite at Buren, displaying internal feldspar clasts with sigmoidal-shape and top-to-the left (west) sense-of-shear. Location: 69º43'13N, 18º37'2E. e) Thin-section image of the mylonitic texture in EG-III granite at Buren (figure 13d). Sigmoidal and recrystallized quartz lenses are enclosed within a matrix of white mica and biotite, and mica-fishes oblique to the shear zone define S-C structure. Image is oriented W-E and in cross-polarized light.

Figure 14. a) Steep D3 ductile shear zone with internal, red-colored EG-IV granite pegmatite, arranged as a sheet truncating subhorizontal (presumed EG-I) sills. Locality; Senja shear belt. 69º27'35''N, 18º11'21''E b) Close-up horizontal view of the shear zone in 14a, showing EG-IV granite with ductile foliation, lens-shaped K-feldspar clasts, and a mica-rich matrix. c) Steep D3 shear zone inside Ersfjord Granite sills at Hatten. 69º40'48''N, 18º33'12''E. Note EG-I sills drag-folded sinistrally into the shear zone boundaries. View is to the north. d) Horizontal view of a discordant EG-III pegmatite granite dyke in foliated TTGs. The dyke is D3 folded and transposed into a steep D3

shear zone. Locality; Kvalsund shear zone. e) Thin-section image of EG-IV granite in D3 mylonitic shear zone in Ersfjord Granite at Hatten. Note epidote and albite grains defining asymmetric lenses oriented in an S-C texture, enclosed by a biotite-rich matrix, in cross-polarized light.

Fig. 15. Schematic geotectonic evolution and emplacement model for the 1.80-1.75 Ga Ersfjord Granite suite and the Senja granitoids in the WTBC, and their relation to the Lofoten-Vesterålen TIB-1 Magmatic Suite in a SW-NE diagrammatic transect (modified after Bergh et al., 2010, 2015). a) Pre-collisional stage (1.80-1.784 Ga) with subduction southwest of Lofoten, then delamination of the mafic lower crust and intrusion of voluminous TIB-1 magmas in Lofoten AMCG-suite (Laurent et al., 2029). Farther northeast 2.4-2.0 Ga rift-basins started to close in between Neoarchaean crustal fragments in WTBC. Extension in back-arcs on Senja and Kvaløya generated large volumes of Ersfjord Granite melts, intruded as EG-1 sills, using Senja shear belt and Kvalsund shear zone as melt pathways. b) Syn-orogenic SW-NE crustal shortening (1.78-1.774 Ga), imbricate nappe thrusting/ stacking, and recumbent folding of arc-related crustal blocks (D1-event) in an evolving accretionary setting. Renewed EG-II Ersfjord Granite melts intruded using EG-1 sills and migmatite pendants as melt pathways. c) Late-tectonic (1.774-1.745 Ga) accretion and coaxial, regional macro-folding (D2-event) followed by orogen-parallel shortening and transpression (D3 event) (Bergh et al., 2010), when the crust uplifted, and terranes fully amalgamated. EG-III and EG-IV granite pegmatite dykes and sills intruded as axial-planar dykes and thrusts in D2 folds, and along subvertical D3 fold limbs and steep D3 strike-slip shear zones, in the vicinity of Senja shear belt and Kvalsund shear zone. Abbreviations: Ab=Astridal belt, KSZ=Kvalsund shear zone, MSB=Mjelde-Skorelvvatn supracrustal belt, RGb= Ringvassøya greenstone belt, Svb= Svanfjellet supracrustal belt, Ssb=Senja shear belt, Tb=Torsnes supracrustal belt, Vg=Vanna Group.

Table 1. Summary characteristics of injected Ersfjord Granite magmas in WTBC, termed EG-I to V, and including previous age dating results (from Corfu et al., 2003; Armitage and Bergh, 2005; Bergh et al., 2010, 2015; Myhre et al., 2013; Laurent et al., 2019), structural characteristics, metamorphism, tectonic setting, and tectonic-induced melt emplacement (this work).

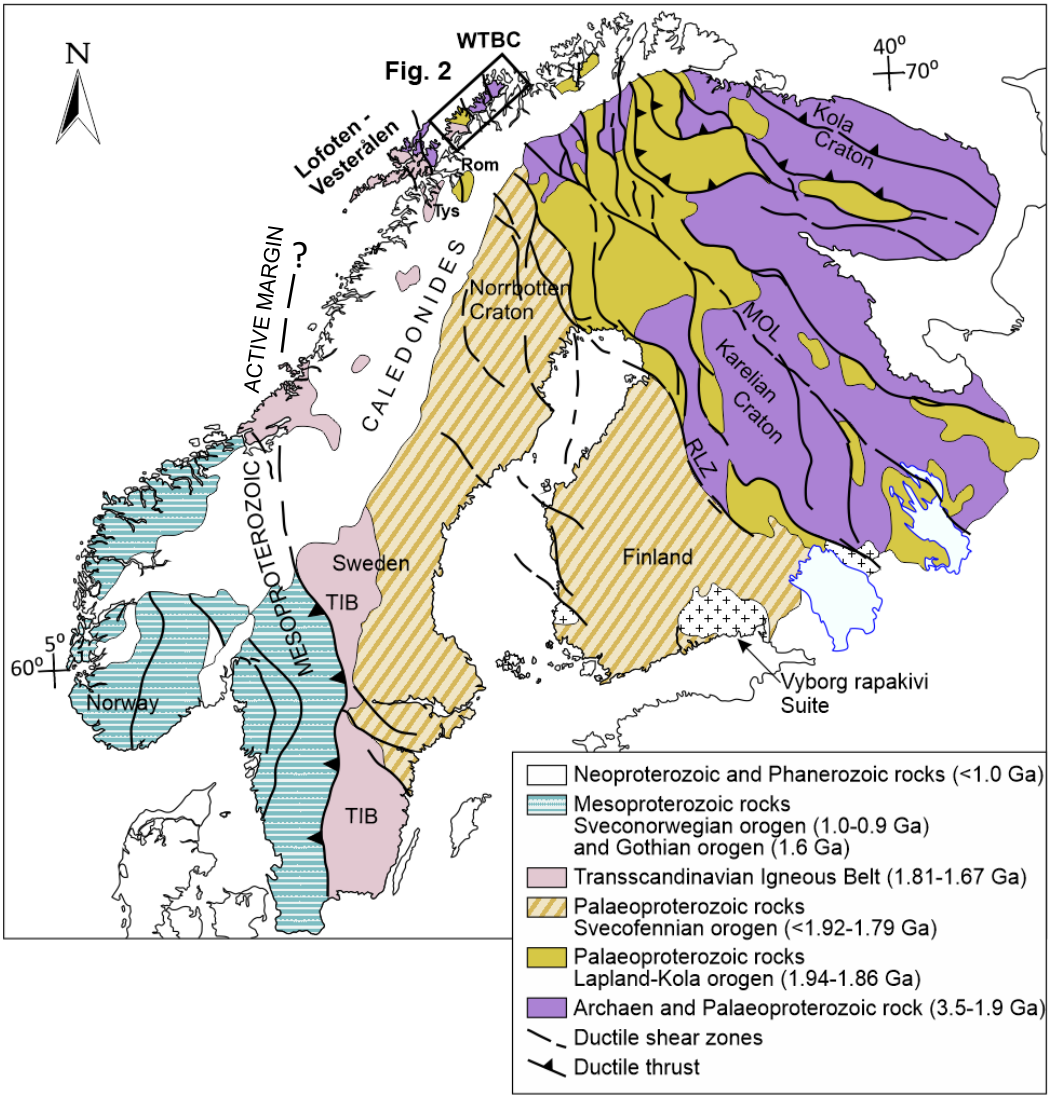
N
WTBC
Fig. 2
Lofoten - Vesterålen
Rom
Tys
ACTIVE MARGIN ?
CALEDONIDES
MESOPROTEROZOIC
Norrbotten Craton
Kola Craton
MOL
Karelian Craton
RLZ
Sweden
TIB
TIB
Finland
Norway
Vyborg rapakivi Suite
40°
70°
5°
60°
Neoproterozoic and Phanerozoic rocks (<1.0 Ga)
Mesoproterozoic rocks
Sveconorwegian orogen (1.0-0.9 Ga)
and Gothian orogen (1.6 Ga)
Transscandinavian Igneous Belt (1.81-1.67 Ga)
Palaeoproterozoic rocks
Svecofennian orogen (<1.92-1.79 Ga)
Palaeoproterozoic rocks
Lapland-Kola orogen (1.94-1.86 Ga)
Archaen and Palaeoproterozoic rock (3.5-1.9 Ga)
Ductile shear zones
Ductile thrust

Figure 1.

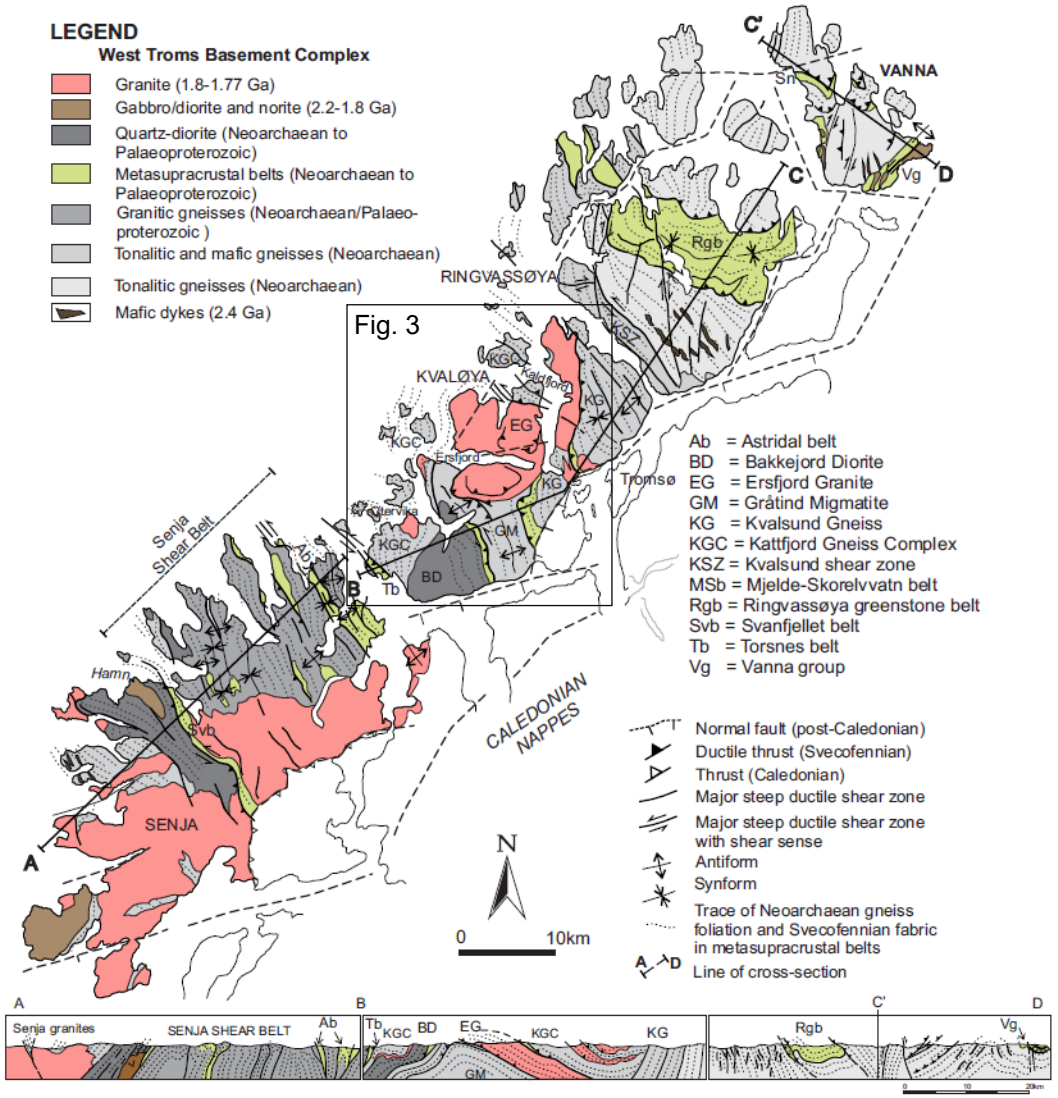
LEGEND
West Troms Basement Complex
Granite (1.8-1.77 Ga)
Gabbro/diorite and norite (2.2-1.8 Ga)
Quartz-diorite (Neoarchaean to Palaeoproterozoic)
Metasupracrustal belts (Neoarchaean to Palaeoproterozoic)
Granitic gneisses (Neoarchaean/Palaeo-proterozoic)
Tonalitic and mafic gneisses (Neoarchaean)
Tonalitic gneisses (Neoarchaean)
Mafic dykes (2.4 Ga)
Fig. 3
VANNA
RINGVASSØYA
KVALØYA
Tromsø
Ersfjord
Kaldfjord
Kåfjord
Kvitvika
Senja Shear Belt
SENJA
Hamn
Svb
CALEDONIAN NAPPES
Ab = Astridal belt
BD = Bakkejord Diorite
EG = Ersfjord Granite
GM = Gråtind Migmatite
KG = Kvalsund Gneiss
KGC = Kattfjord Gneiss Complex
KSZ = Kvalsund shear zone
MSb = Mjelde-Skorelvvatn belt
Rgb = Ringvassøya greenstone belt
Svb = Svanfjellet belt
Tb = Torsnes belt
Vg = Vanna group
Normal fault (post-Caledonian)
Ductile thrust (Svecofennian)
Thrust (Caledonian)
Major steep ductile shear zone
Major steep ductile shear zone with shear sense
Antiform
Synform
Trace of Neoarchaean gneiss foliation and Svecofennian fabric in metasupracrustal belts
Line of cross-section
N
0
10km
Senja granites
SENJA SHEAR BELT

Figure 2.

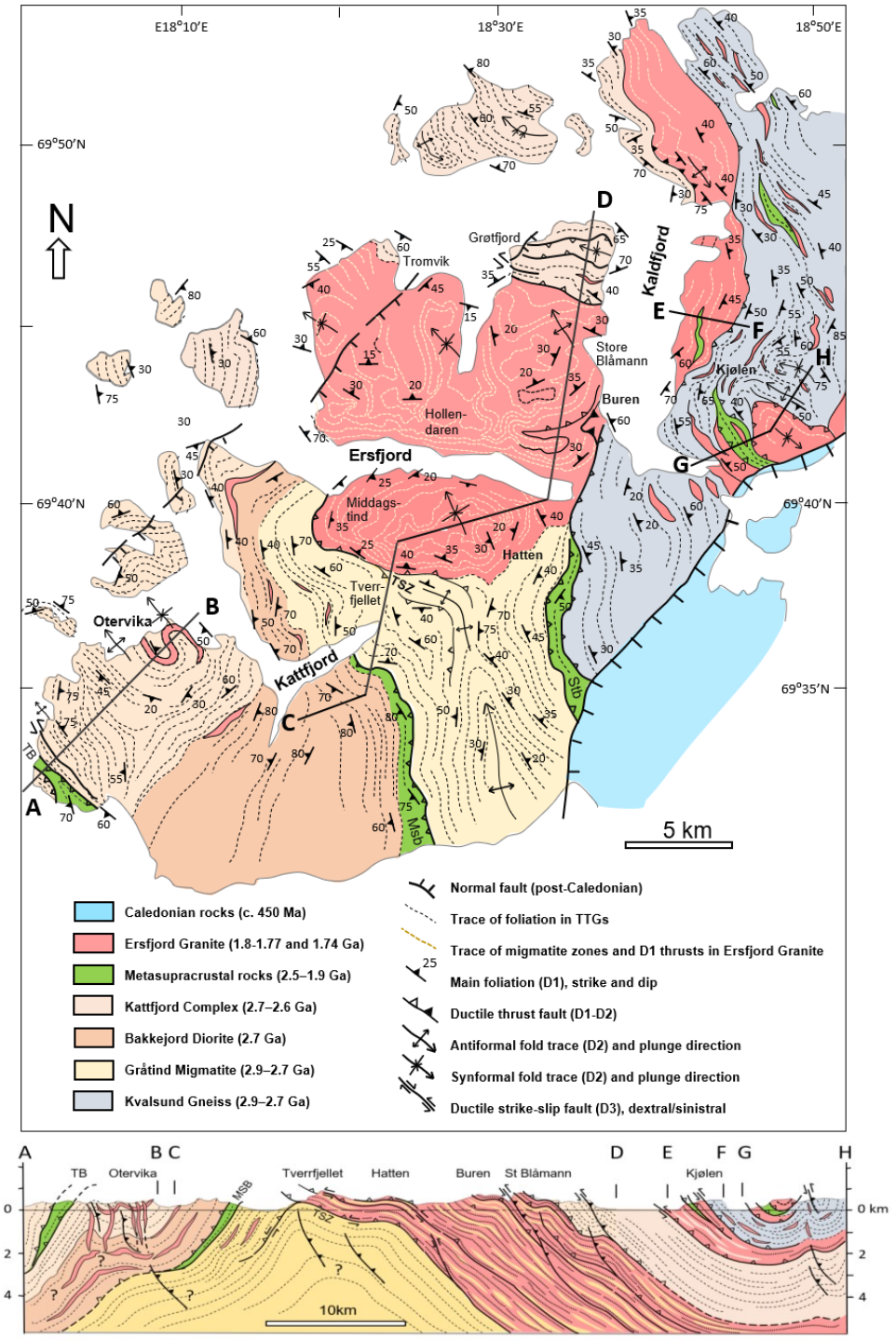
E18°10′E
18°30′E
18°50′E
69°50′N
69°40′N
69°35′N
N
Tromvik
Grøtfjord
Kaldfjord
Store Blåmann
Kjølen
Buren
Hollen-daren
Ersfjord
Middags-tind
Hatten
Tverr-fjellet
TSZ
Otervika
Kattfjord
TB
MSB
A
B
C
D
E
F
G
H
5 km
Caledonian rocks (c. 450 Ma)
Ersfjord Granite (1.8-1.77 and 1.74 Ga)
Metasupracrustal rocks (2.5–1.9 Ga)
Kattfjord Complex (2.7–2.6 Ga)
Bakkejord Diorite (2.7 Ga)
Gråtind Migmatite (2.9–2.7 Ga)
Kvalsund Gneiss (2.9–2.7 Ga)
Normal fault (post-Caledonian)
Trace of foliation in TTGs
Trace of migmatite zones and D1 thrusts in Ersfjord Granite
Main foliation (D1), strike and dip
Ductile thrust fault (D1-D2)
Antiformal fold trace (D2) and plunge direction
Synformal fold trace (D2) and plunge direction
Ductile strike-slip fault (D3), dextral/sinistral
A
B C
D
E
F G
H
TB
Otervika
MSB
Tverrfjellet
Hatten
Buren
St Blåmann
Kjølen
TSZ
0
2
4
0 km
2
4
10km

Figure 3.

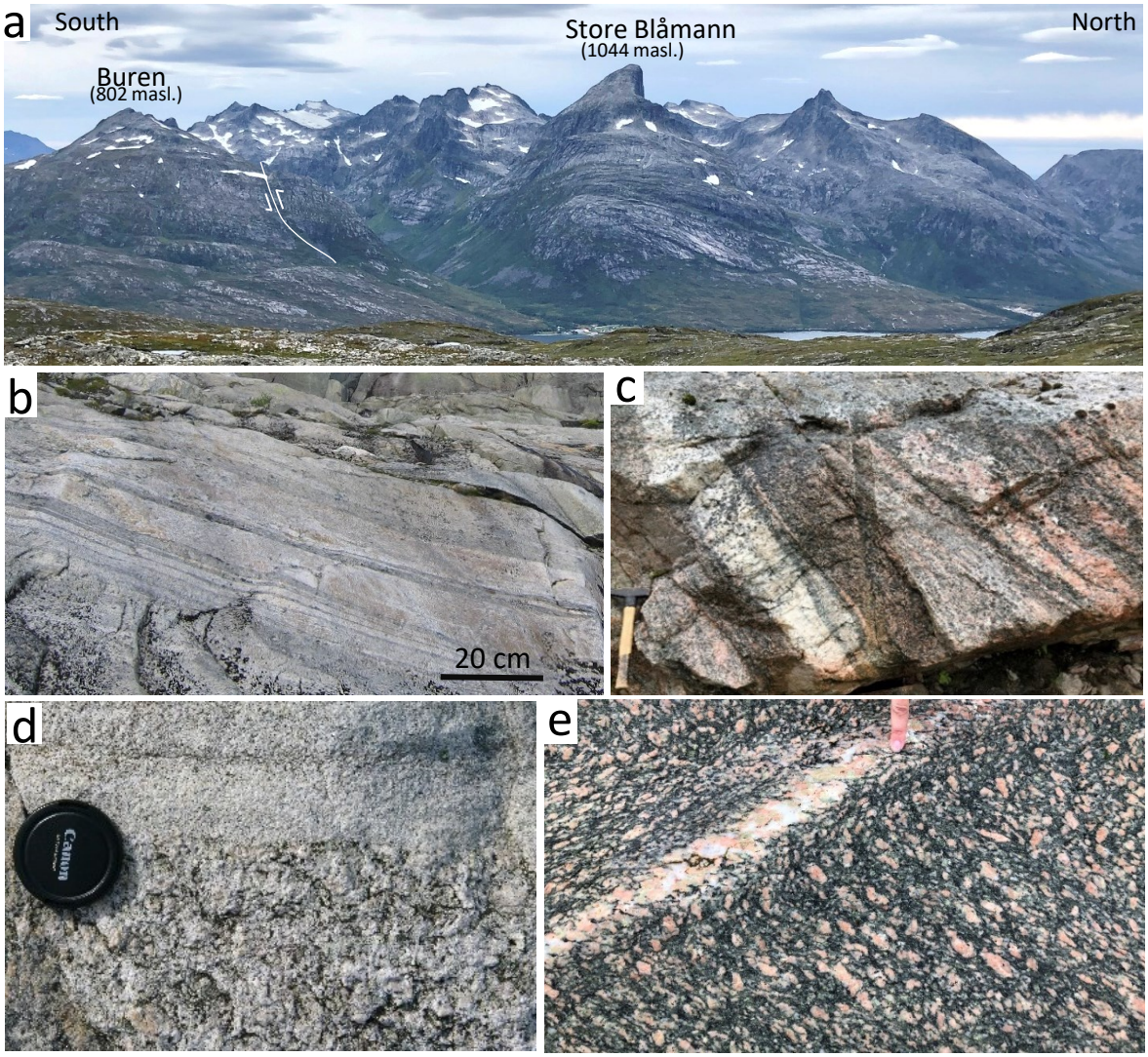
a
South
Store Blåmann
(1044 masl.)
North
Buren
(802 masl.)
b
20 cm
c
d
e

Figure 4.

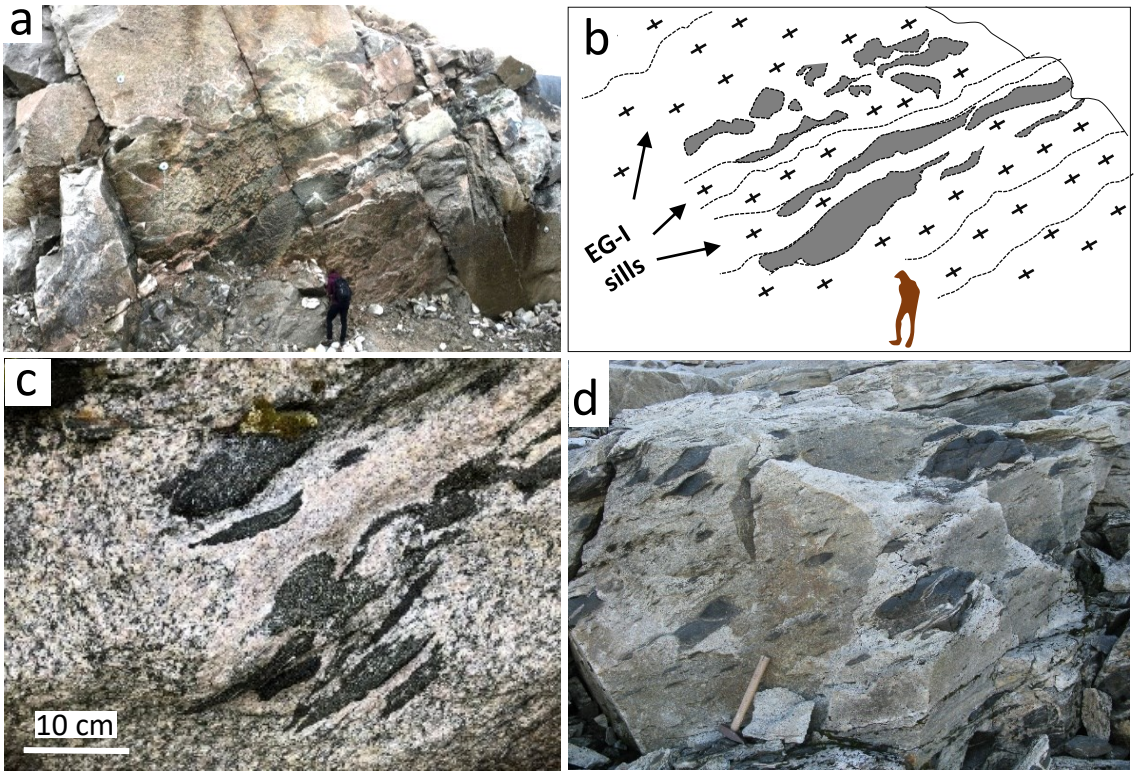

Figure 5.

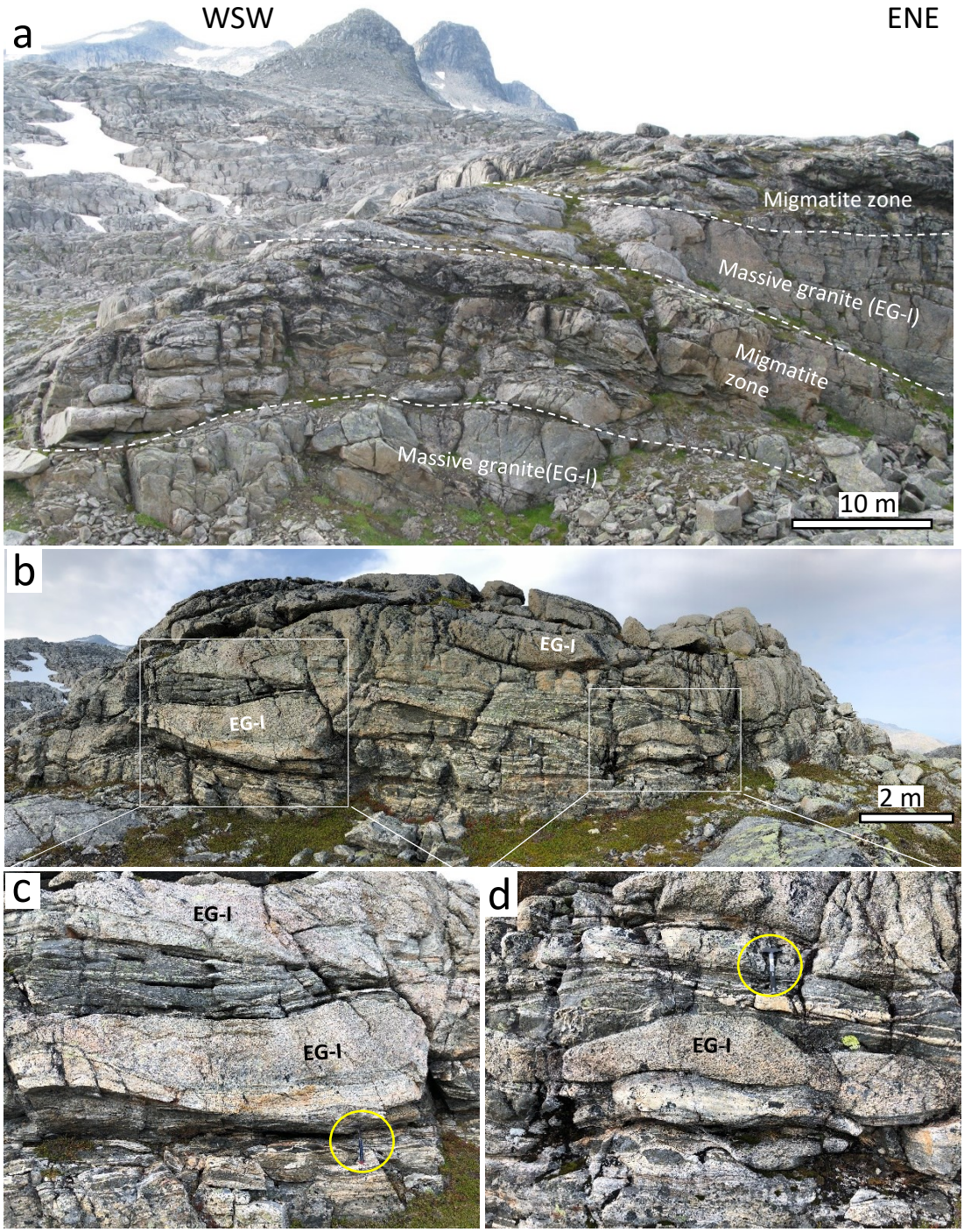
a
WSW
ENE
Migmatite zone
Massive granite (EG-I)
Migmatite zone
Massive granite(EG-I)
10 m
b
EG-I
EG-I
2 m
c
EG-I
EG-I
d
EG-I

Figure 6.

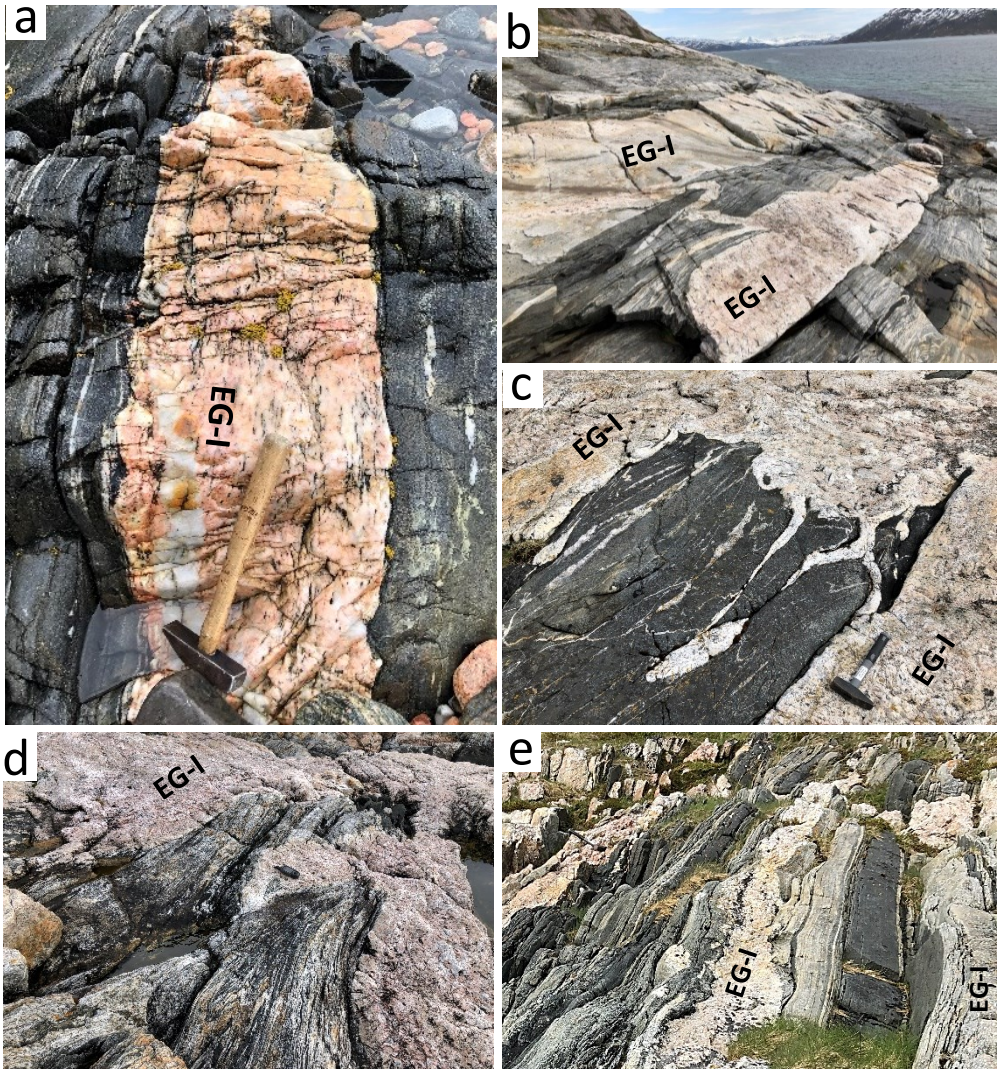

Figure 7.

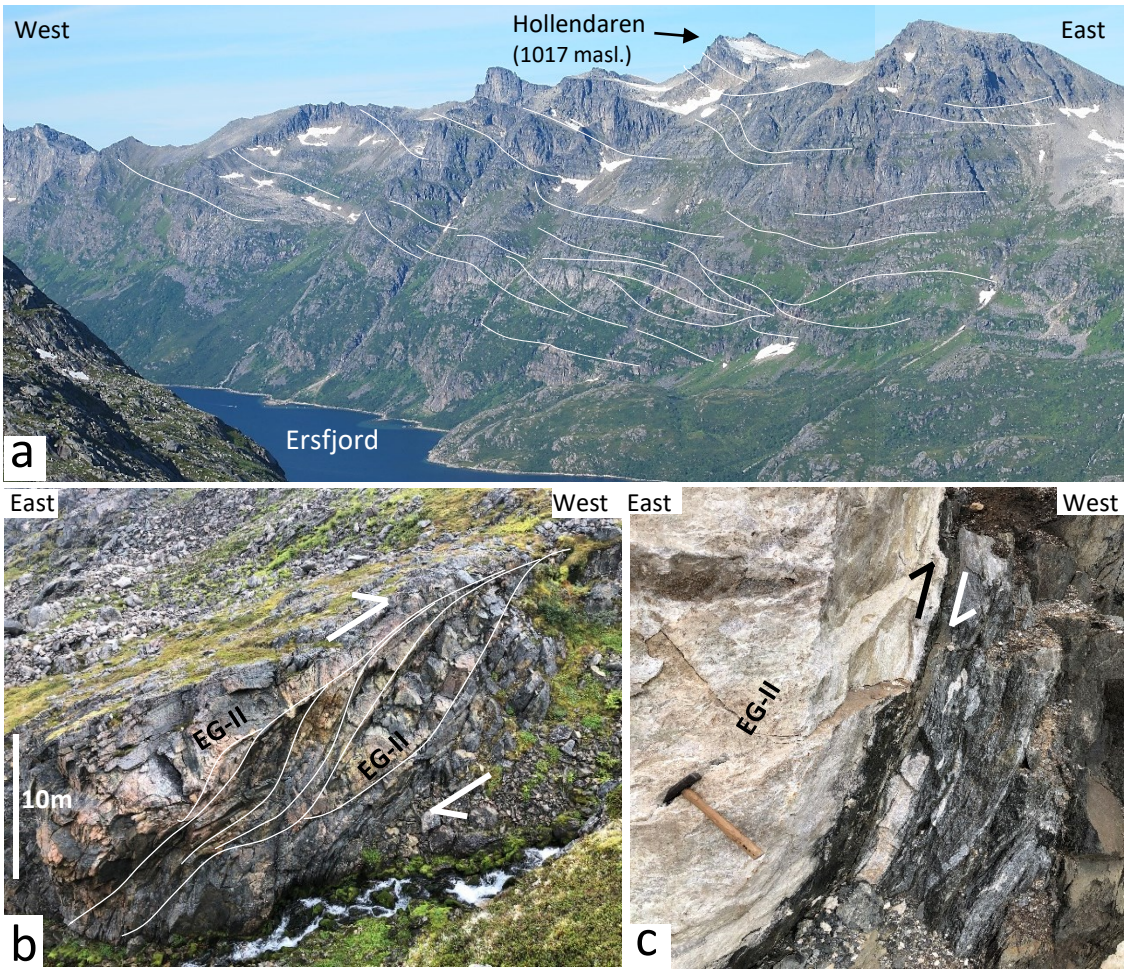
West
Hollendaren
(1017 masl.)
East
Ersfjord
a
East
West
EG-II
EG-II
10m
b
East
West
EG-II
c

Figure 8.

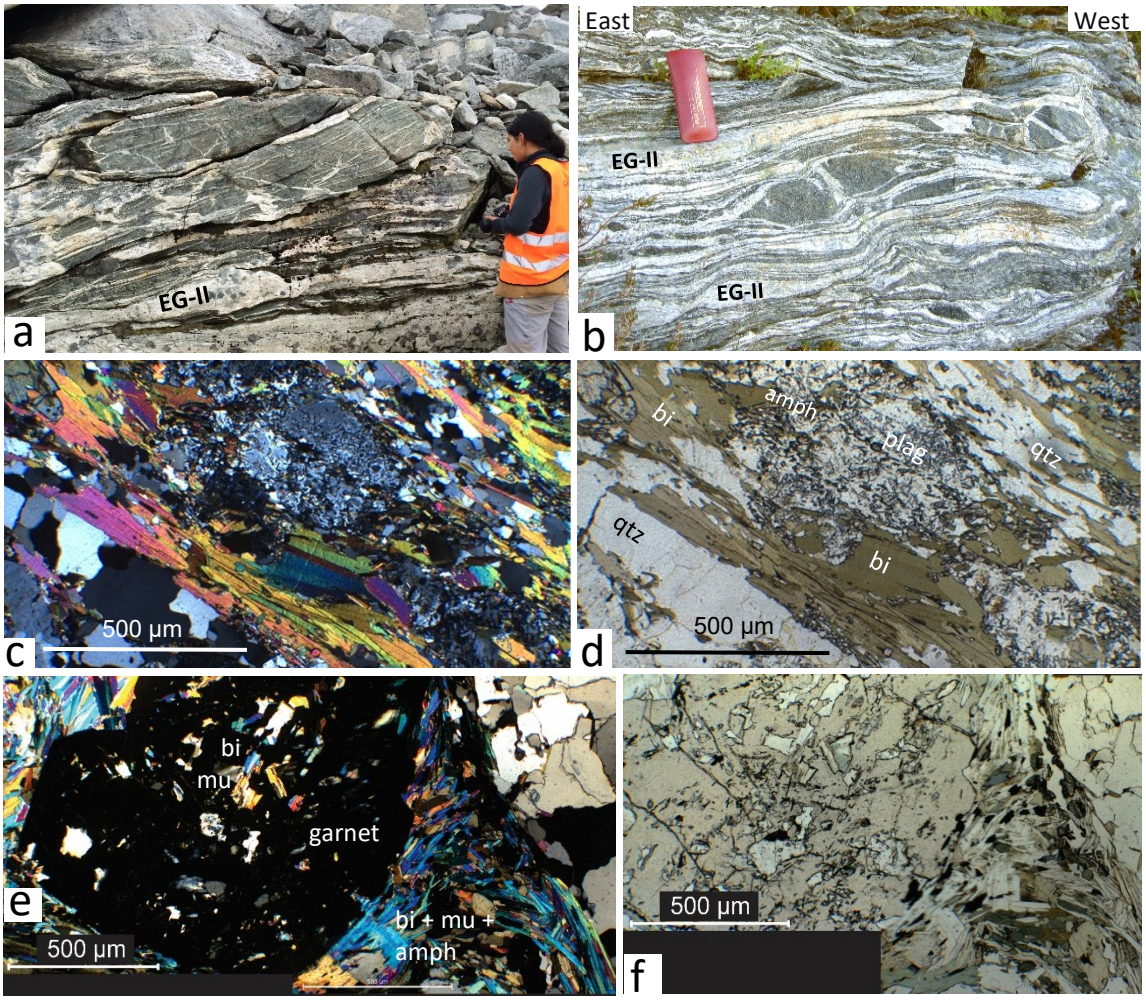
a
EG-II
East
West
EG-II
EG-II
b
c
500 µm
bi
amph
plag
qtz
qtz
bi
500 µm
d
bi
mu
garnet
bi + mu +
amph
500 µm
e
500 µm
f

Figure 9.

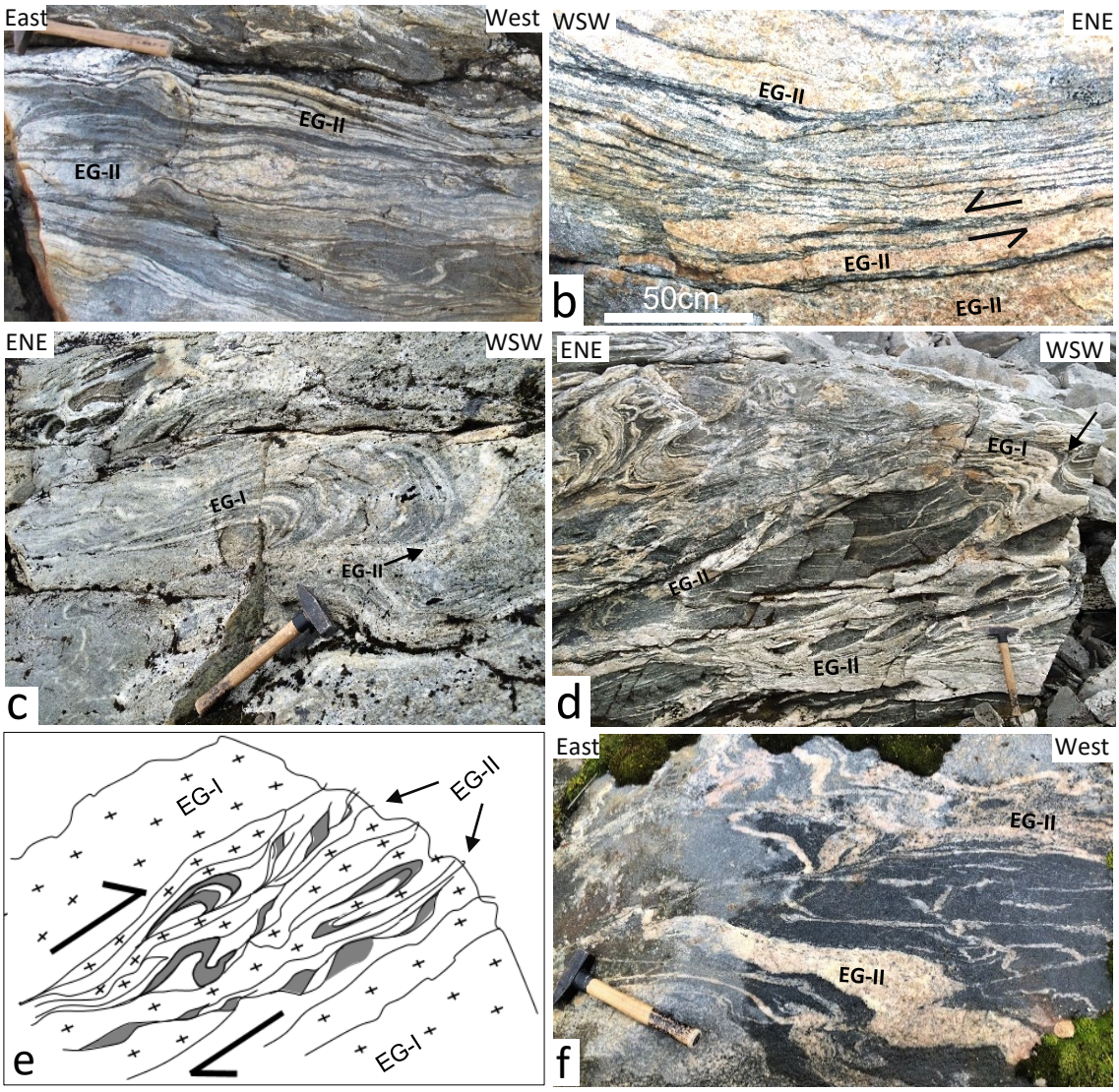
East
West
EG-II
EG-II
WSW
ENE
EG-II
EG-II
EG-II
50cm
b
ENE
WSW
EG-I
EG-II
c
ENE
WSW
EG-I
EG-II
EG-II
d
EG-I
EG-II
EG-I
e
East
West
EG-II
EG-II
f

Figure 10.

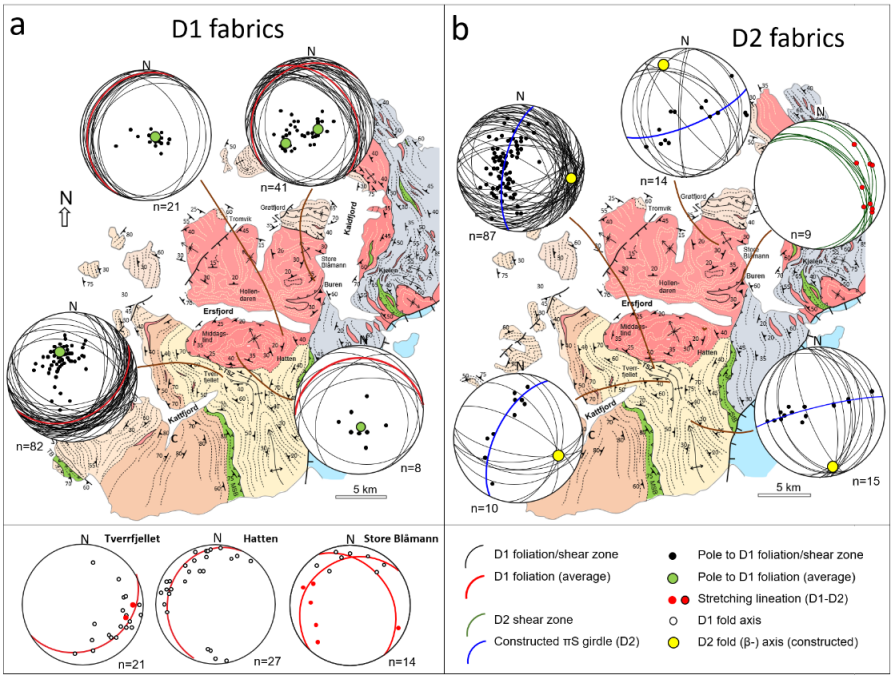
a
D1 fabrics
b
D2 fabrics
N
n=21
n=41
n=82
n=8
n=87
n=14
n=9
n=10
n=15
5 km
Ersfjord
Kattfjord
Tverrfjellet
Hatten
Store Blåmann
n=21
n=27
n=14
D1 foliation/shear zone
D1 foliation (average)
D2 shear zone
Constructed πS girdle (D2)
Pole to D1 foliation/shear zone
Pole to D1 foliation (average)
Stretching lineation (D1-D2)
D1 fold axis
D2 fold (β-) axis (constructed)

Figure 11.

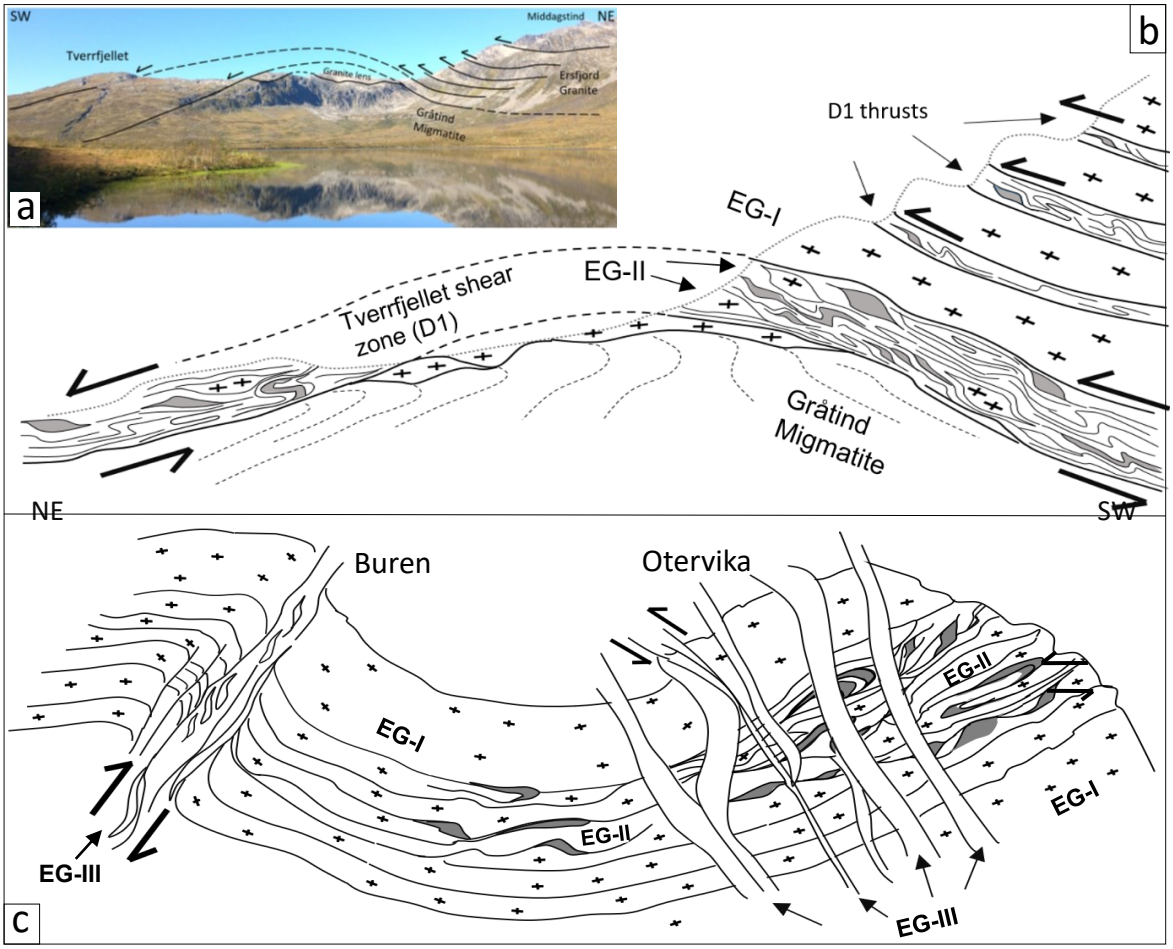
SW
Middagstind
NE
Tverrfjellet
Granite lens
Ersfjord Granite
Gråtind Migmatite
a
b
D1 thrusts
EG-I
EG-II
Tverrfjellet shear zone (D1)
Gråtind Migmatite
NE
SW
Buren
Otervika
EG-I
EG-II
EG-III
EG-II
EG-I
EG-III
c

Figure 12.

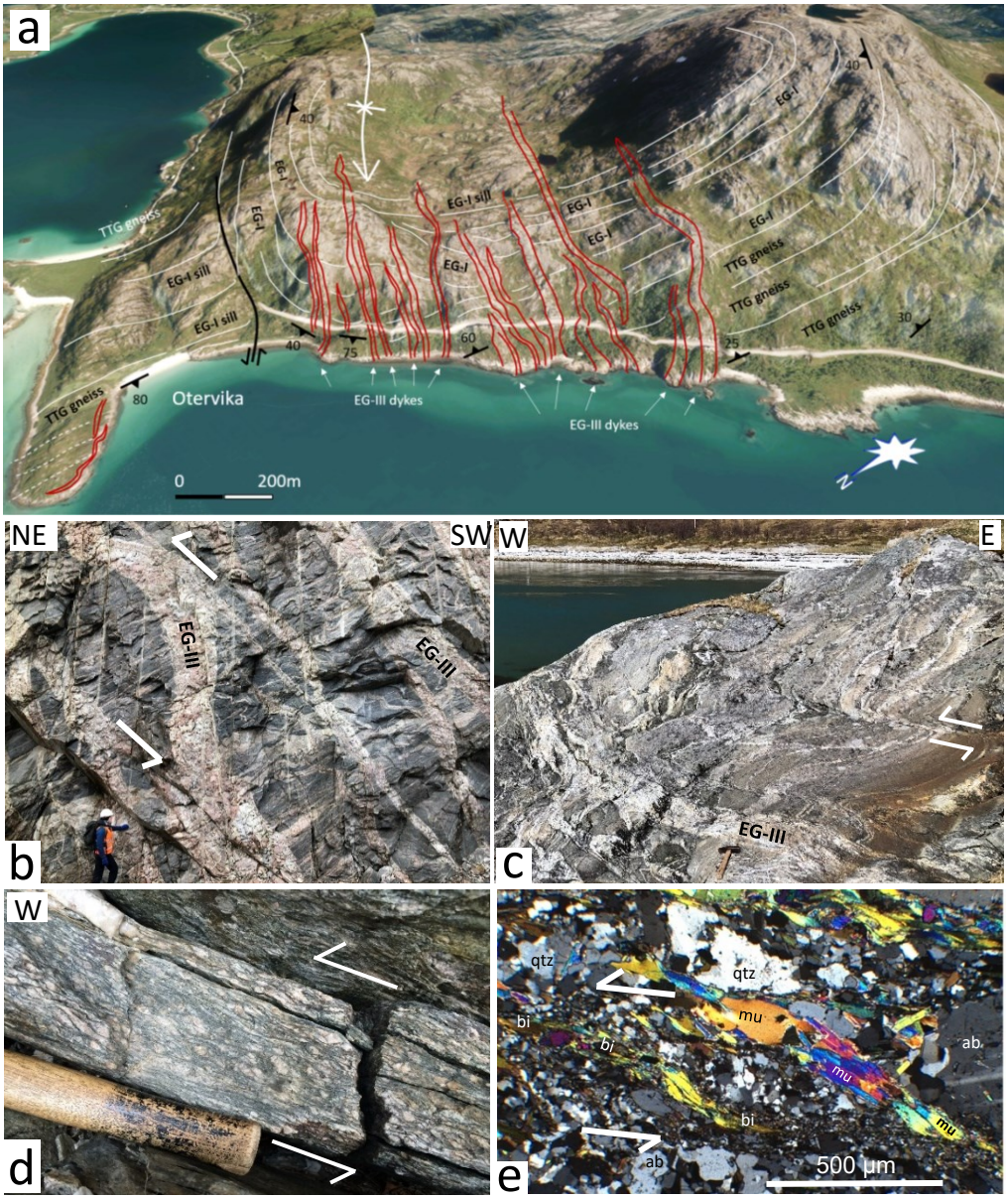
a
TTG gneiss
EG-I sill
EG-I
EG-I sill
EG-I
EG-I sill
EG-I
EG-I
EG-I
TTG gneiss
TTG gneiss
TTG gneiss
TTG gneiss
Otervika
EG-III dykes
EG-III dykes
40
40
75
60
80
25
30
0
200m
N
NE
SW
EG-III
EG-III
b
W
E
EG-III
c
W
d
qtz
qtz
bi
bi
mu
mu
mu
ab
ab
bi
500 µm
e

Figure 13.

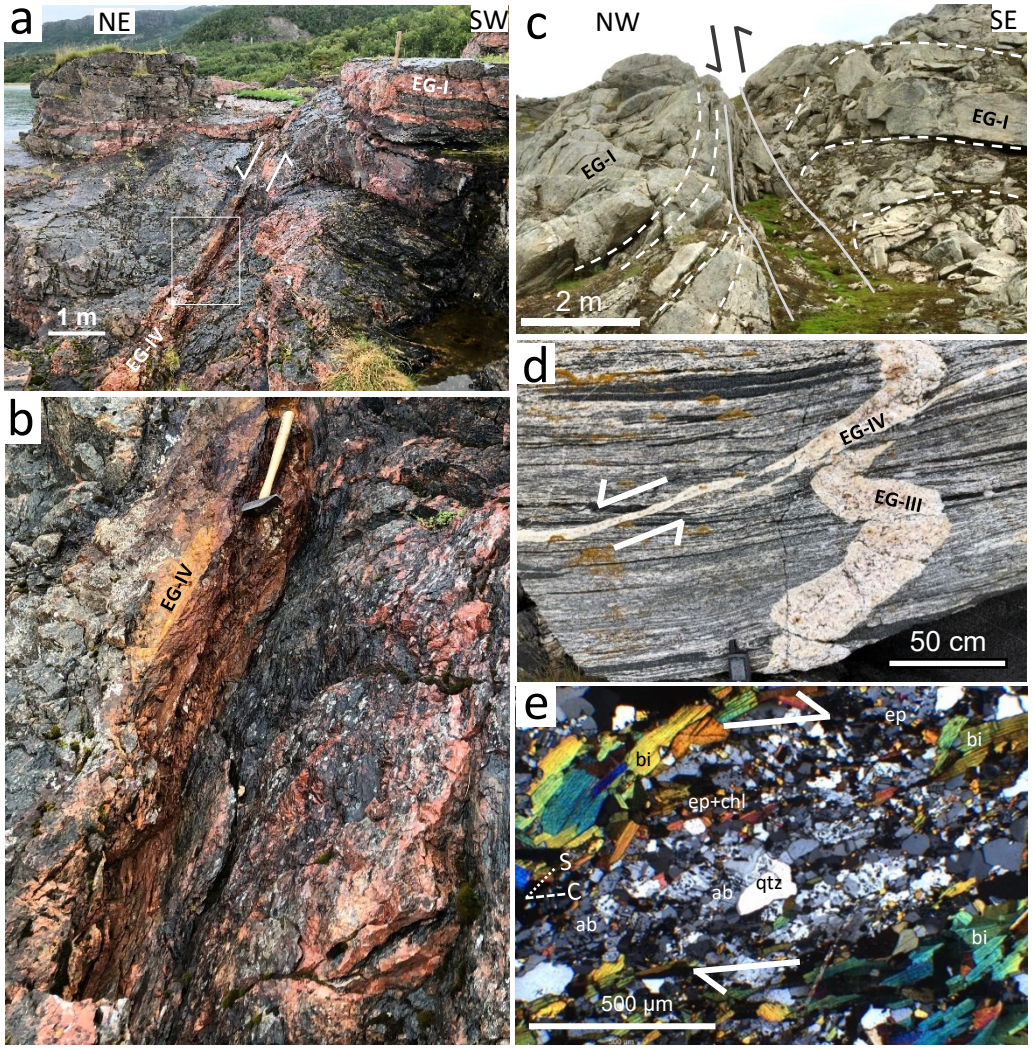
a
NE
SW
EG-I
1 m
EG-IV
b
EG-IV
c
NW
SE
EG-I
EG-I
2 m
d
EG-IV
EG-III
50 cm
e
ep
bi
bi
ep+chl
S
C
ab
qtz
ab
bi
500 µm

Figure 14.

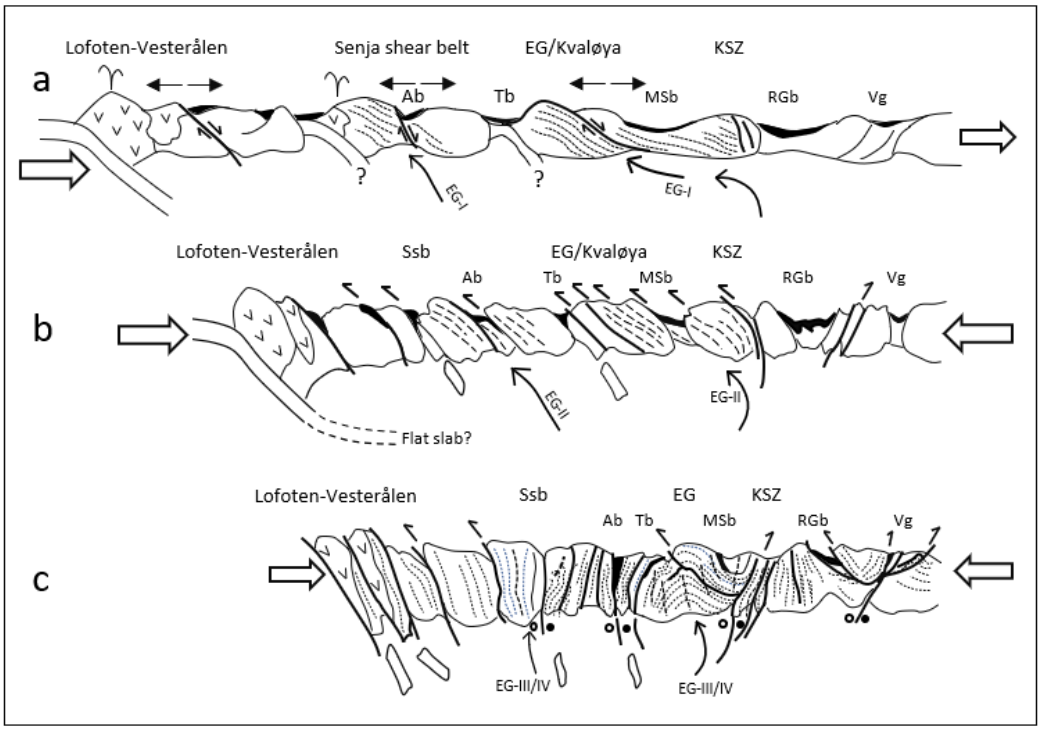
a
Lofoten-Vesterålen
Senja shear belt
EG/Kvaløya
KSZ
Ab
Tb
MSb
RGb
Vg
?
?
EG-I
EG-I
b
Lofoten-Vesterålen
Ssb
EG/Kvaløya
KSZ
Ab
Tb
MSb
RGb
Vg
EG-II
EG-II
Flat slab?
c
Lofoten-Vesterålen
Ssb
EG
KSZ
Ab
Tb
MSb
RGb
Vg
EG-III/IV
EG-III/IV

Figure 15.

Intrusion	**Absolute ages** (Kvaløya, Senja)	**Structure, kinematics & contact relations**	**Metamorphic grade** (mineral assemblage)	**Tectonic setting**	**Structural evolution and melt emplacement**
EG-I (pre-D1)	1792 ±5 Ma 1798-1784 Ma	- Regional sheets/sills - Pervasive magmatic banding - Conformable mafic migmatite zones (pendants) - Intrusive, sharp contacts	Primary igneous minerals: K-fsp + plag + qtz + amph + bi + mu ± epidote/ allanite, ti, magn, ap, zr	Pre-collisional extension in back-arc setting	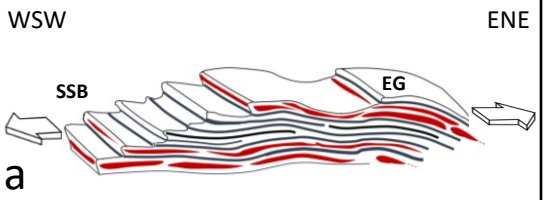
EG-II (syn-D1)	1784-1775 Ma (?) 1758 Ma	- Foliation-parallel sills - West-directed nappe stack - Imbricate ductile thrusts - Recumbent isoclinal and west-vergent folds - Stretching lineation	Amphibolite facies (prograde): Amph + garnet + bi + mu + Kfsp + plag + qtz	- Syn-orogenic NE-SW crustal shortening - Basement-involved fold-thrust nappes - Accretionary orogen (advancing)	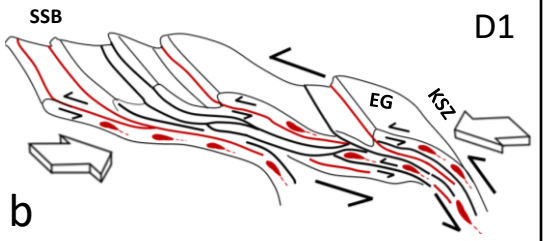
EG-III (syn-D2)	1774 ±5 Ma 1769 ±3 Ma	- Steep, axial-planar dykes (granite pegmatites) - Intrusive and thrust contacts - Regional upright folds - Mylonitic thrusts with top west shear-sense - Sigma-/mica fish/S-C bands	Low amphibolite to upper greenschist facies (retrograde): Epidote + sericite + saussuritized plag + bi + mu + Kfsp + qtz	- Continued coaxial orogenic shortening relative to D1 - Accretion and crustal uplift	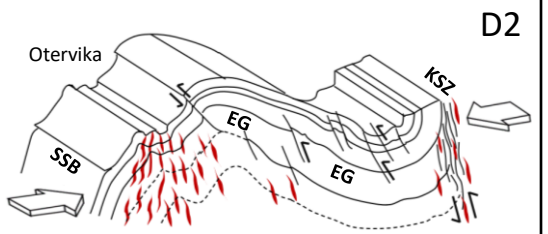
EG-IV (syn-D3)	1751 ±8 Ma 1745 Ma	- Steep dykes and sills - Sharp intrusive contacts - Subvertical folds - Steep mylonitic shear zones - Transpressive ductile shear zones (oblique/strike-slip) - Sinistral & dextral shearing	Greenschist facies (retrograde): Bi + mu + epidote + chlorite + saussitized-/ sericitized plag + qtz + Kfsp	- Late-orogenic NW-SE oblique shortening - Strike-slip shearing - Transpressive accre-tionary orogen - Crustal uplift	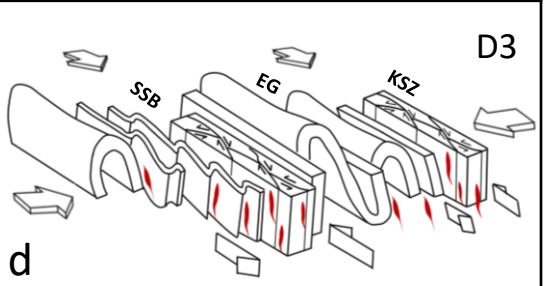
EG-V (post-D3)	1633-1562 Ma	- Irregular clusters and dykes - Intrusive contacts		Post-orogen reworking and rejuvenation	